Organic Geochemistry 186 (2023) 104705

Contents lists available at ScienceDirect

Organic Geochemistry

journal homepage: www.elsevier.com/locate/orggeochem

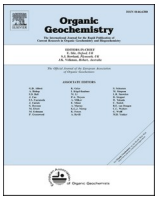

The biological source and paleoenvironment implication of rare short-chain lanostanes in alkaline lacustrine sediments

Dongyong Wang [a], Meijun Li [a,b,*], Jianfa Chen [a], Hong Xiao [a], Xianli Zou [b], Lu Yang [c], Haochen Chen [a], Huiqiang Qin [a]

[a] National Key Laboratory of Petroleum Resources and Engineering, China University of Petroleum (Beijing), Beijing 102249, China
[b] Faculty of Petroleum, China University of Petroleum-Beijing at Karamay, Karamay, Xinjiang 834000, China
[c] College of Resources and Environment, Chengdu University of Information Technology, Chengdu 610225, China

ARTICLE INFO

Associate Editor — John K. Vollman

Keywords:
Molecule markers
Lanostanes
Alkaline lakes
Cyanobacteria
Hypersaline water body
Fengcheng formation
Junggar Basin

ABSTRACT

Highly mature organic-rich source rocks in the Early Permian Fengcheng Formation, Mahu Sag, Junggar Basin, northwestern China, were deposited in an alkaline lacustrine environment. Analysis of extracts of eight core samples by gas chromatography–mass spectrometry detected a series of short-chain lanostanes (C_{23}–C_{25}) lanostanes. The relative abundance of short-chain lanostanes has a strong positive correlation with those of long chain (C_{30}–C_{32}) homologues, indicating a possible common biological origin and genesis. Compound specific isotopic analyses of phytane, steranes, hopanes and C_{30} lanostane from the core extracts reflect input from primary photosynthetic producers including cyanobacteria. Abundant lamalginite was observed in the samples from the study area. A well-defined positive relationship is also evident between the relative abundance of lanostanes and the ratios of 7-+8-methyl heptadecanes/C_{max} and 2-methyl hopanes/C_{30}-hopanes. Given that 7-+8-methyl heptadecanes and 2-methyl hopanes are considered to be diagnostic molecular biomarkers for organic matter derived from cyanobacteria, it is possible that cyanobacteria may serve as a possible biological precursor for lanostanes in the Fengcheng Formation. The influence of maturity on the lanostanes is considered to be minor, as no significant relationship is found between lanostanes and thermal maturity parameters, although this may be due to a limited maturity range of the samples. The co-existence of high contents of phytane, β-carotanes, and gammacerane, and their correlations in abundance with lanostanes, indicates a strongly reducing sedimentary environment.

1. Introduction

Steroids occur widely in ancient sediment extracts and crude oils (Huang and Meinschein, 1976, 1979; Peters et al., 2005). The C_{27}, C_{28} and C_{29} regular steranes are extensively used to determine organic matter sources and sedimentary environment (Huang and Meinschein, 1979) and therefore are applied to oil-source correlation (Bechtel et al., 2014). Compared with regular steranes, lanostanes are rarely reported in sediment extracts and oils. Using gas chromatography–mass spectrometry (GC–MS) and co-injection of synthetic standards, long chain (C_{30}–C_{32}) lanostanes were identified for the first time in saline source rocks and tar sands from the Biyang Sag (Chen et al., 1989, 1990; Chen and Summons, 2001). The C_{30} and C_{31} lanostanes also have been positively identified following a series of isolation and derivatization procedure and desulfurization of C_{30} and C_{31} lanostane sulfides in low mature oil samples (Peng et al., 1998). C_{30}–C_{32} lanostanes had previously been detected in ancient marine limestones and Cambrian deposits (Parfenova, 2011; Bhattacharya et al., 2021). The consensus was been that C_{30} lanostane forms from C_{30} lanosterol, which is derived from C_{30} squalene (Chen et al., 1989), with the lanosterol receiving methyl substituents at the positions of C_4 and C_{14} atoms in the A- and C- rings (Summons et al., 2006). Lu et al. (2011) first reported the short-chain C_{24} and C_{25} lanostanes in crude oils with high sulfur contents from the Bohai Bay Basin. As lanostanes have been detected in mostly source rocks and oils formed under marine, saline or high-sulfur environments, they are considered to be molecular markers for hypersaline depositional environments that are useful for oil-source correlation in such conditional settings. (Wang et al., 2021a).

Up to now, C_{24}–C_{25} lanostanes have been identified only in crude oils and little work has been done on the origin of lanostanes. Here, we

* Corresponding author at: 18 Fuxue Road, Changping District, Beijing 102249, China.
E-mail address: meijunli@cup.edu.cn (M. Li).

https://doi.org/10.1016/j.orggeochem.2023.104705
Received 22 July 2023; Received in revised form 7 November 2023; Accepted 7 November 2023

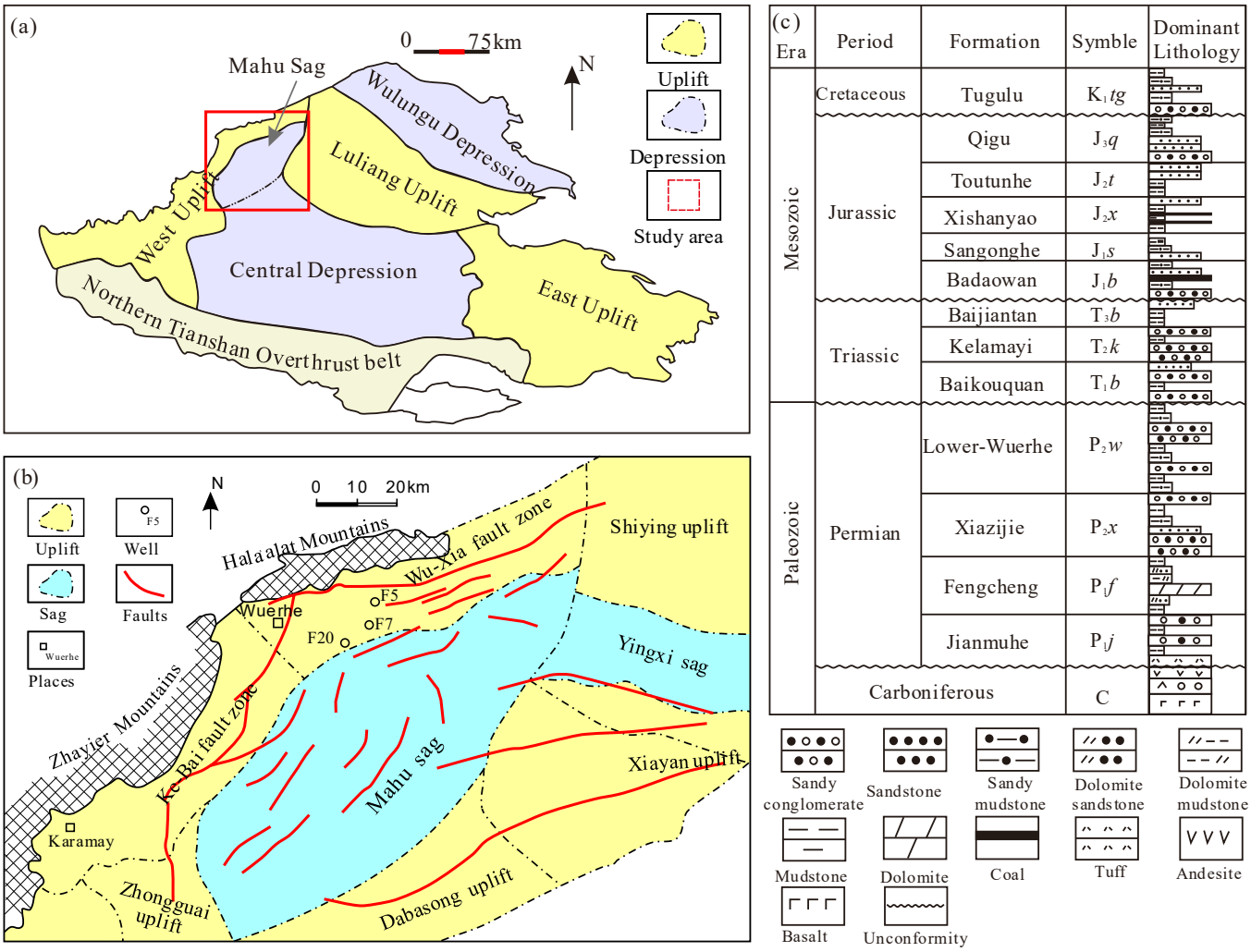

Fig. 1. Map showing the geological setting, stratigraphic column, and the location of wells F5, F7 and F20 in the Mahu Sag, Junggar Basin, NW China.

report on the occurrence and identification of C_{23}–C_{25} lanostanes in alkaline dolomitic mudstone from the Mahu Sag and investigate their origins.

2. Geologic setting

The Junggar Basin is one of the most important petroliferous basins in northwest China (Zhang et al., 1984) and its geologic settings have been reported in many previous studies (e.g., Lee, 1985; Wang et al., 2019; Tang et al., 2021a). It is a superimposed basin with sediments more than 5 km thick that has experienced multiple tectonic movements since the Late Paleozoic. The basin is divided, from south to north, into the Southern Margin Thrust Belt, Western Uplift, Central Depression, Eastern Uplift, Luliang Uplift and Wulungu Depression (Fig. 1a). The Mahu Sag, with an area of 3000 km^2, is located in the northwestern part of the Central Depression (Fig. 1a). The study area is dominated by NE-SW trending faults, with some NW-SE faults (Fig. 1b). Four major erosional events have resulted in key regional unconformities (Ma et al., 2015) (Fig. 1c). The stratigraphy of the Mahu sag is comprised of several marine, continental and transitional sequences. Carboniferous strata were deposited in a marine environment, following by approximately one km of lower Permian marine and continental transitional sediments.

Table 1
Basic information and geochemical data for selected core samples.

Sample ID	Well	Depth (m)	Lithology	TOC (%)	S_1 (mg/g TOC)	S_2 (mg/g TOC)	HI (mg/g TOC)	VR (%Ro)	Sat (%)	Aro (%)	NSO (%)	Asp (%)
F1	F5	3214.70	Dolomitic mudstone	0.64	0.40	2.49	390	0.96	48.8	23.8	22.6	4.8
F2	F5	3226.90	Dolomitic mudstone	1.30	0.36	6.96	537	1.11	40.3	21.2	37.6	0.9
F3	F5	3233.38	Dolomitic mudstone	1.02	0.65	6.15	602	1.14	55.0	26.7	13.1	5.2
F4	F5	3249.50	Dolomitic mudstone	1.01	0.35	5.37	531	/	66.7	21.2	11.4	0.7
F5	F5	3288.70	Dolomitic mudstone	1.21	0.26	7.07	583	/	51.9	38.7	6.7	2.7
F6	F5	3354.20	Dolomitic mudstone	1.22	0.32	9.08	744	1.01	64.4	22.8	12.5	0.3
F7	F7	3189.29	Dolomitic mudstone	2.93	1.66	25.7	877	/	94.0	4.0	1.7	0.3
F8	F20	3268.00	Dolomitic mudstone	2.40	2.73	20.1	836	/	47.9	41.2	10.7	0.2

Notes: TOC: total organic matter content; S_1: volatile hydrocarbon (HC) content; S_2: remaining (HC) generative potential; HI: Hydrogen index = $S_2 \times 100$/TOC; VR: vitrinite reflectance; Sat: the relative content of saturated hydrocarbon; Aro: the relative content of aromatic hydrocarbon; NSO: the relative content of non-hydrocarbon; Asp: the relative content of asphaltene.

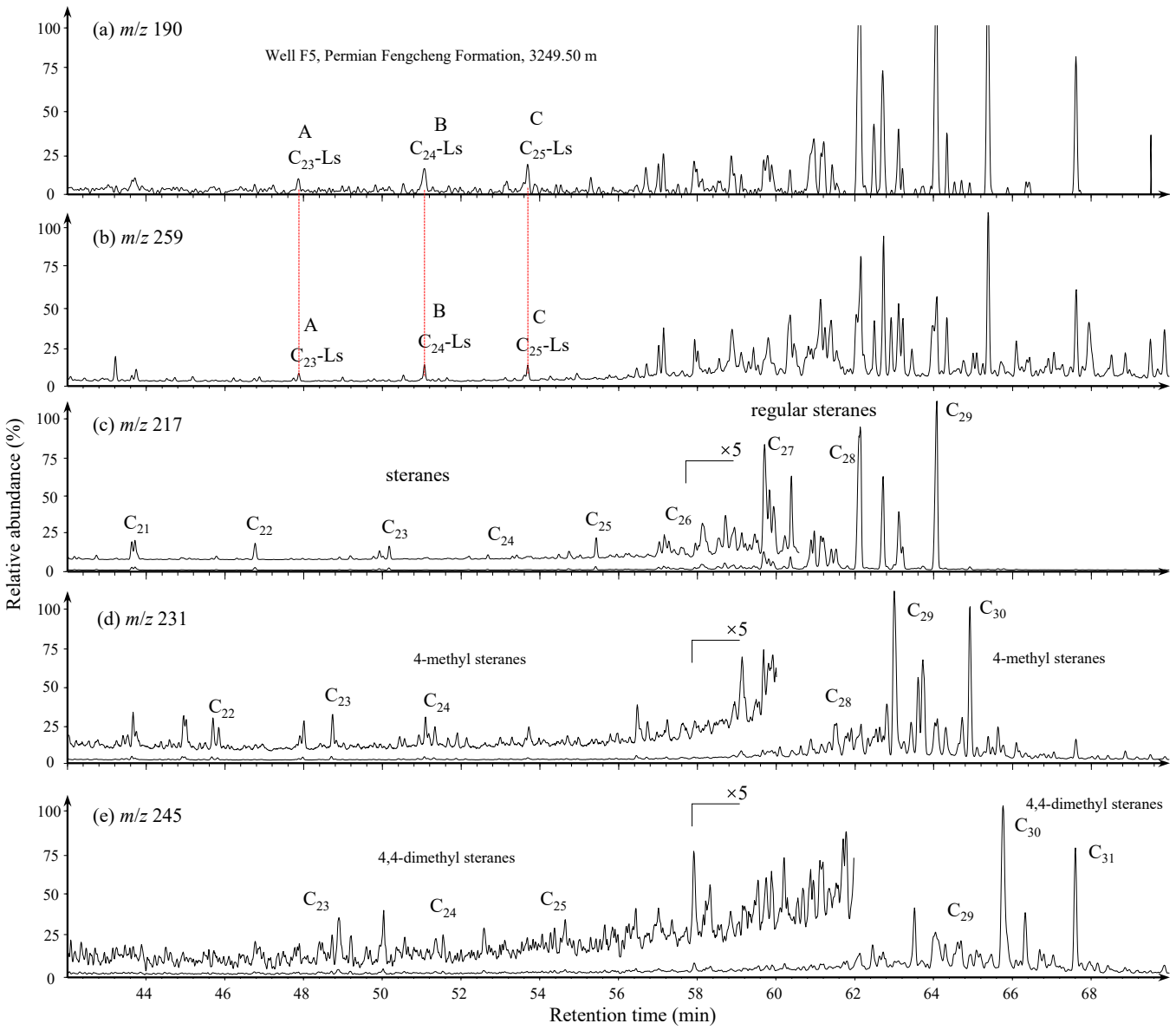

Fig. 2. Representative *m/z* 190, 259, 217, 231 and 245 mass chromatograms in Fengcheng Formation sediments samples from well F5. Ls: lanostane.

The middle to upper Permian formed almost entirely in continental settings. After the Paleozoic marine and continental transitional sediments, Mesozoic fluvio-lacustrine sediments with an average thickness of three kilometers were deposited (Fig. 1c).

Recently, giant oilfields have been discovered in the conglomerate reservoirs of the Triassic Baikouquan Formation in the Mahu Sag (Kang et al., 2019; Tang et al., 2021b; Yu et al., 2022) (Fig. 1c). The Fengcheng Formation is considered as the source rock for the majority of the discovered oils in the sag (Tao et al., 2019; Xiao et al., 2021; Zhang et al., 2022). The Fengcheng Formation consists of several distinctly different lithofacies assemblages from the central region to margin: carbonate, evaporite-rich lake deposits, siliciclastic alluvial deposits, and volcanic ash deposits (Wang et al., 2021b). Significant amounts of alkaline minerals, including wegscheiderite, trona (Yu et al., 2018), reedmergnerite, searlesite (Guo et al., 2021) and chert (Yu et al., 2021) are observed in the strata, indicating deposition in a typical hypersaline water body (Cao et al., 2020; Wang et al., 2021b).

3. Samples and methods

3.1. Samples

Eight cores were sampled from three exploratory wells in the western slope of the Mahu Sag. The locations of the wells are shown in Fig. 1b and basic information for the core samples is listed in Table 1.

3.2. TOC measurement and Rock-Eval pyrolysis

Core samples were ground to less than 80 mesh in a crusher, and inorganic carbonates removed with hydrochloric acid. Total organic carbon (TOC) content was performed by a LECO CS-230 Carbon/Sulfur Analyzer. Rock-Eval pyrolysis analysis was carried out using an OGE-II equipment. The initial temperature was 300 °C (held for 3 min) and then programmed to 600 °C at a rate of 25 °C/min. The volatile hydrocarbon content (S_1) and remaining hydrocarbon generation potential (S_2) were obtained at temperatures of 300 °C and 300–600 °C respectively.

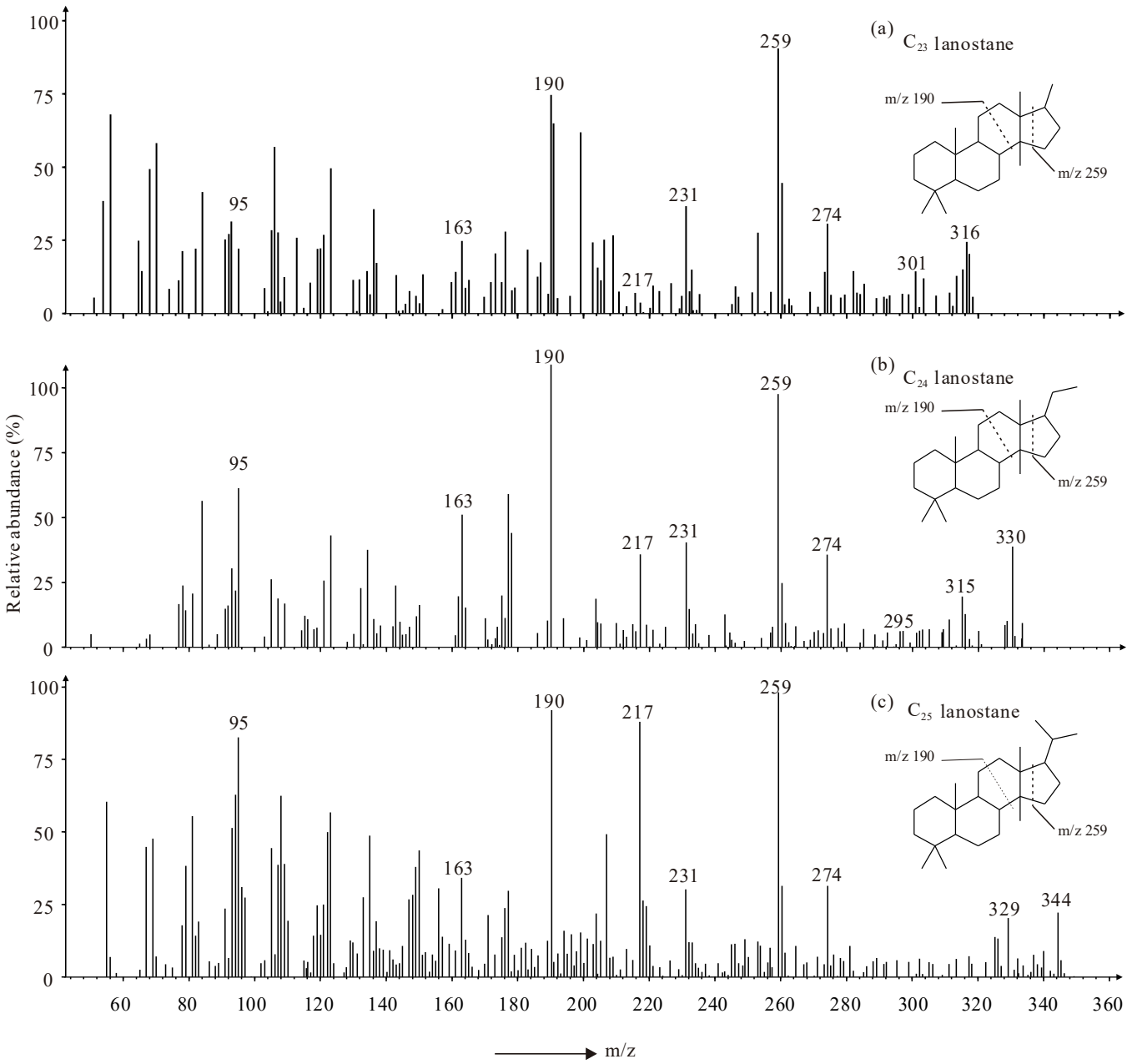

Fig. 3. Mass spectra showing the characteristic ions and molecular ions of C_{23}–C_{25} lanostanes.

3.3. GC–MS analysis

The source rock extracts were obtained using a Soxhlet apparatus, with about 500 mL of dichloromethane solvent. The rock extracts were deasphaltened using about 50 mL of petroleum ether. The collected filtrate was separated into three fractions–saturates, aromatics and resin–using silica gel/alumina (2:1, v/v) columns (10 mm × 150 mm) with 60 mL of petroleum ether, 40 mL of a mixture of dichloromethane and petroleum ether (2:1, v/v), and 30 mL of a mixture of dichloromethane and methanol solution (93:7, v/v), respectively.

The GC–MS analysis of the saturate fractions was conducted using an Agilent 6890-5975A, equipped with an HP-5MS (60 m × 0.25 mm × 0.25 μm film thickness) fused silica capillary column. The oven was programmed with an initial temperature of 50 °C held for one min, raised to 120 °C at a rate of 20 °C/min then to 310 °C at 3 °C/min and finally held at 310 °C for 20 min. The mass spectrometer was used in the electron-impact mode with an electron energy of 70 eV. Helium with 99.999 % purity was used as carrier gas. Data were obtained using selected ion monitoring and full scan modes.

3.4. Organic petrography

The cores were cut perpendicular to the bedding, solidified by epoxy resin, ground and polished on an EcoMet 250 equipped with an AutoMet 250 to obtain smooth section surface. Maceral composition observation and vitrinite reflectance determination were performed using a Leica DM4500 microscope equipped with a CRAIC photometer and a 50 × oil immersion objective. The vitrinite reflectance measurements were calibrated by standard materials with known reflectance values (Sapphir, 0.589 %Ro, Gadolinium-Gallium-Garnet, 1.725 %Ro, Cubic Zirconia, 3.08 %Ro and Strontium Titanate, 5.36 %Ro). Over 20 vitrinite reflectance point counts were obtained for each sample.

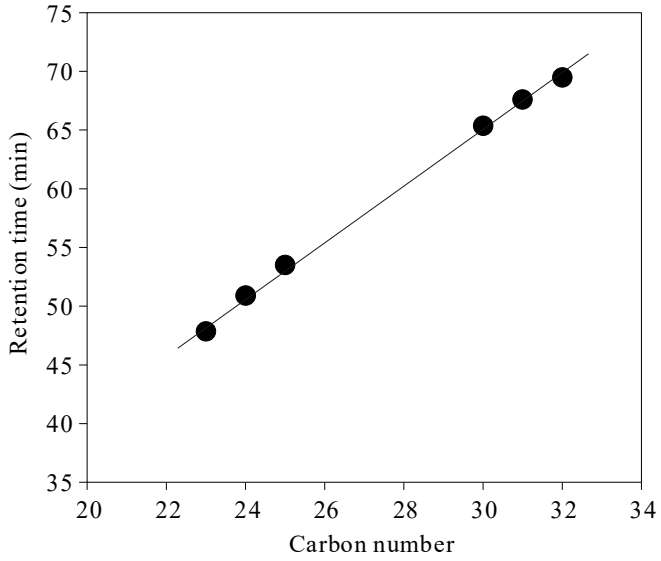

Fig. 4. Cross plot of carbon number of lanostanes and retention times.

3.5. GC–IRMS

The saturated hydrocarbons were separated into normal alkanes and isoalkanes by urea adduction. The compound-specific isotopes were carried out by gas chromatography–isotope ratio mass spectrometer (GC–IRMS). The 7890 gas chromatograph was equipped with a HP-5MS fused silica capillary column (30 m × 0.25 mm × 0.25 μm). The carrier gas is helium (purity > 99.999 %) with a rate of 1.0 mL/min. The GC system initial oven temperature was 100 °C (held for 1 min) programmed at 5 °C/min to 300 °C and held for 20 min. The isotope ratio mass spectrometer was taken in the electron-impact mode with an electron energy of 70 eV. The temperature of combustion oven (including CuO and Pt wires) was 850 °C. The mass range was set to 1–96 Da at a 90 min scanning period. The $\delta^{13}C$ data were obtained by integrating the ion currents for masses 44, 45 and 46 from the CO_2 yielded by the oxidation of each compound during the chromatographical separation, after passing through the combustion oven.

4. Results

4.1. Bulk geochemical characteristics of source rocks

The total organic carbon (TOC) contents of source rocks from the study area range from 0.64 % to 2.93 %, with an average of 1.47 % (Table 1), consistent with good to excellent source units (Peters, 1986).

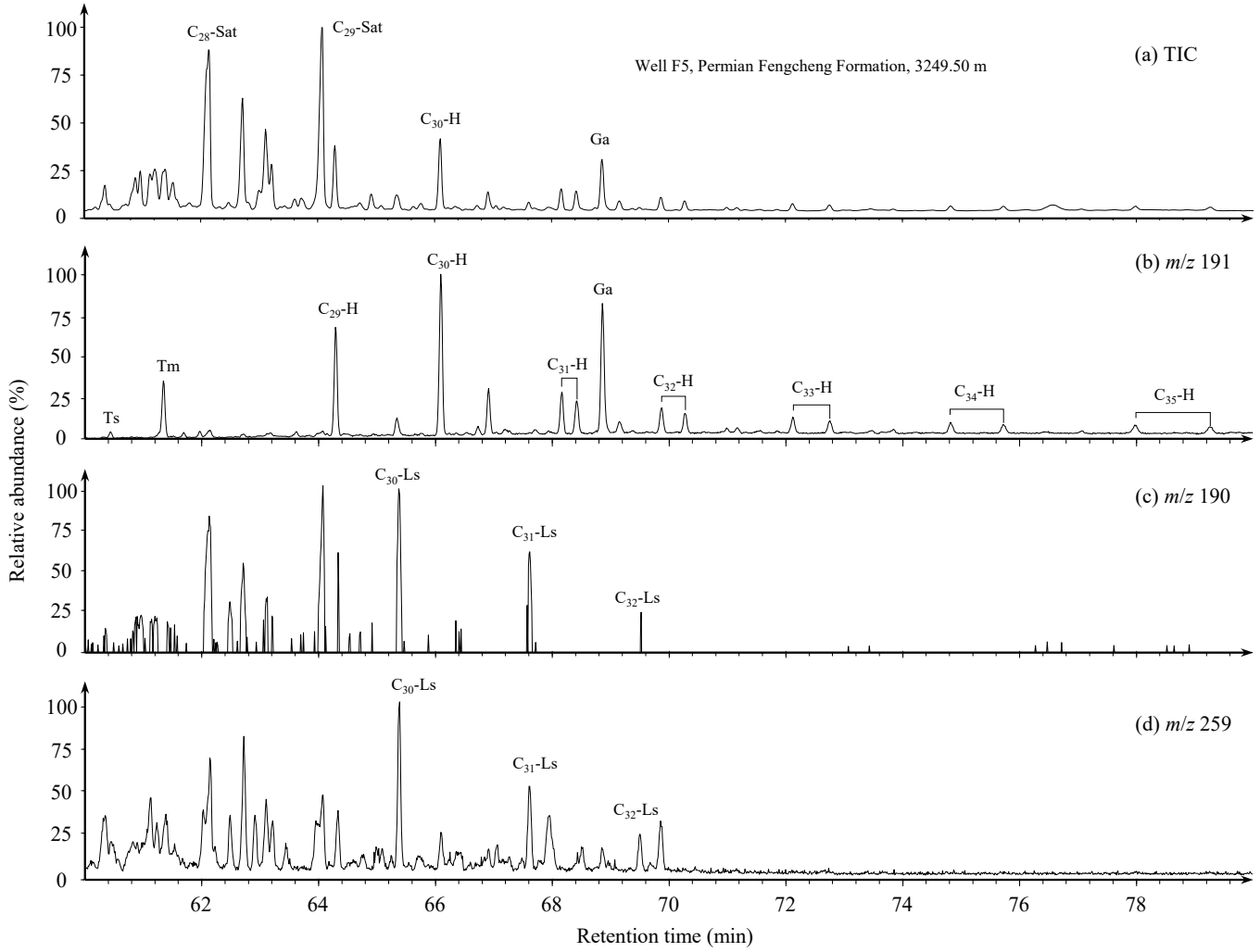

Fig. 5. Representative *m/z* 190, 191, 259 and total ion current (TIC) in Fengcheng Formation sediments samples from well F5. Sat: regular sterane; H: 17α(H),21β(H)-hopane; Ts: 18α(H)-22,29,30-trisnorneohopane; Tm: 17α(H)-22,29,30-trisnorhopane; Ga: gammacerane; Ls: lanostane.

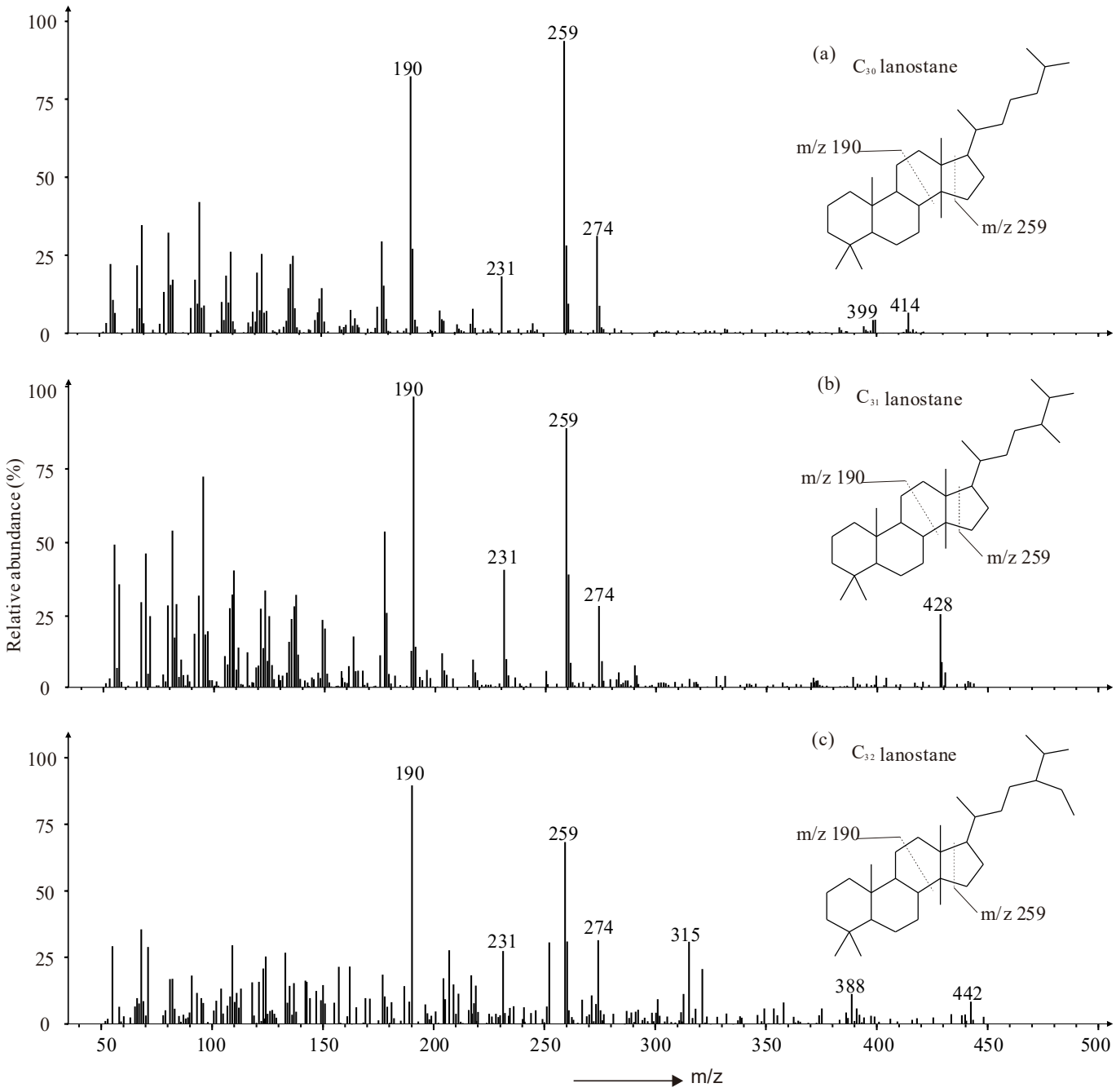

Fig. 6. Mass spectra showing the characteristic ions and molecular ions of C_{30}–C_{32} lanostanes.

The hydrogen indices (HI) range from 390 to 877 mg HC/g TOC and average about 637 mg HC/g TOC, further indicating good to excellent source potential composed predominantly of Type I kerogen (Tissot and Welte, 1984; Espitalié et al., 1985). The vitrinite reflectance (0.96–1.14 %Ro) shows that the organic matter is mature to highly mature.

4.2. Occurrence of C_{23}–C_{25} lanostanes

Lanostanes were detected in *m/z* 190 and *m/z* 259 ion chromatograms of the saturated hydrocarbon fraction extracted from the core samples (Fig. 2a, b). The mass spectra of three compounds are illustrated in Fig. 3, showing their characteristic ions (*m/z* 190 and *m/z* 259), and molecular ions (*m/z* 316, 330, and 344) (Fig. 3). Comparison with mass spectra reported in the literature, peaks B and C, with molecular ions of *m/z* 330 and *m/z* 344, are C_{24} and C_{25} lanostanes, respectively (Lu et al., 2011). The characteristic ions of peak A are *m/z* 190 and *m/z* 259, suggesting that this compound also belongs to the lanostanes series. The molecular weight of peak A is 14 less than C_{24} lanostane and 28 less than C_{25} lanostane, corresponding to one and two fewer carbon atoms, respectively. The retention times of C_{23}–C_{25} and C_{30}–C_{32} lanostanes linearly correlate with their carbon numbers as shown in Fig. 4, further suggesting that compound A is likely C_{23} lanostane.

4.3. Occurrence of C_{30}–C_{32} lanostanes

The C_{30} lanostane, C_{31} lanostane, and C_{32} lanostane elute before C_{30} hopane, C_{31} hopane, and C_{32} hopane, respectively (Fig. 5). As shown in Fig. 6, the characteristic ions of those compounds are *m/z* 190 and 259 and also contain the ions of *m/z* 274, 231 and 217. The molecular weights of the three compounds are 414, 428, and 442, respectively.

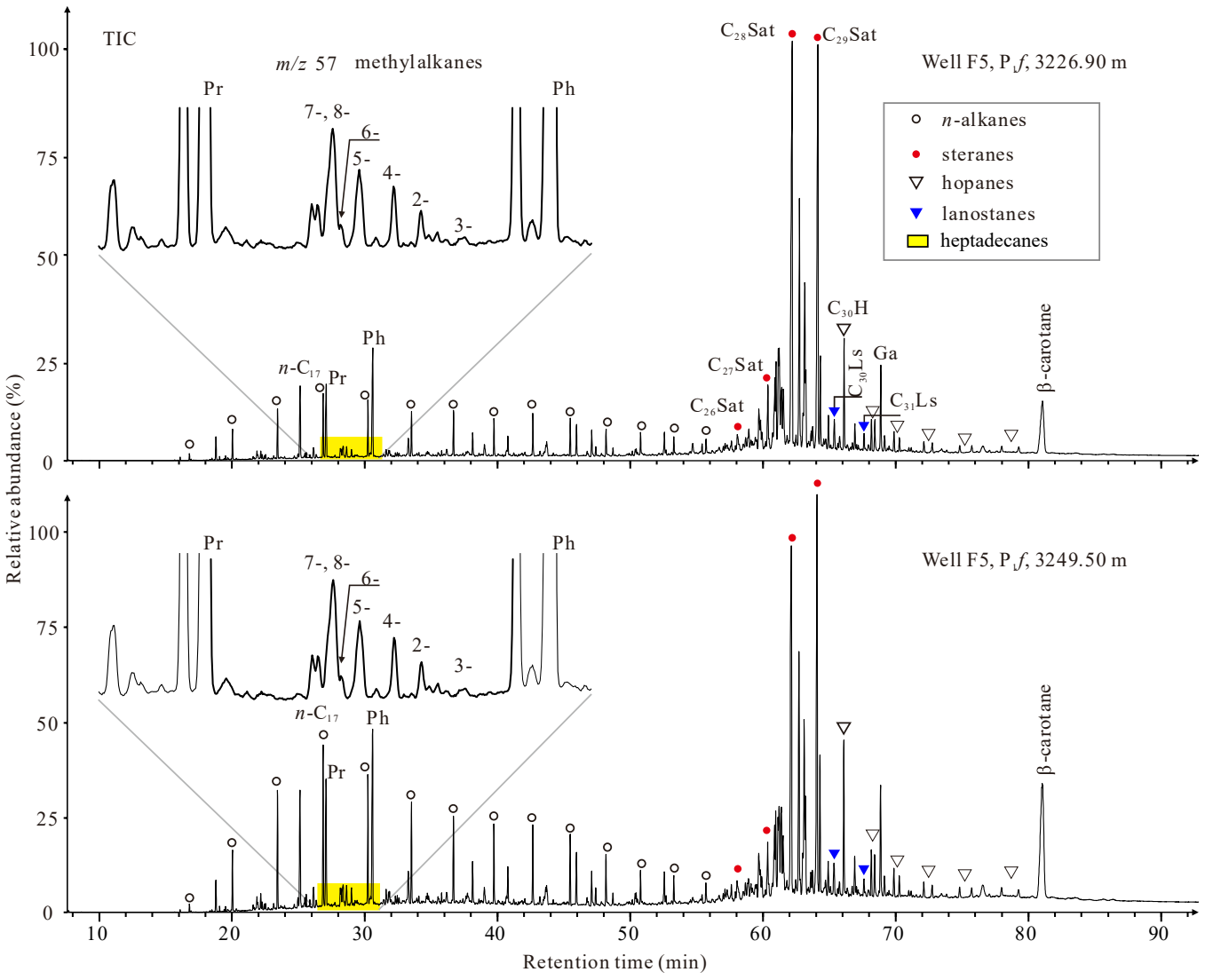

Fig. 7. TICs and *m/z* 57 mass chromatograms of the saturated hydrocarbon fractions of the Fengcheng Formation extracts from well F5. Pr: pristane; Ph: phytane; Sat: regular sterane; H: 17α(H),21β(H)-hopane; Ts: 18α(H)-neohopane; Ga: gammacerane; Ls: lanostane; 2- – 8-: the different positions of methyl group on heptadecanes.

These three compounds are unequivocally identified as C_{30} lanostane, C_{31} lanostane, and C_{32} lanostane by comparison with the mass spectra and relative retention times reported in the literature (Chen et al., 1989; Peng et al., 1998; Lu et al., 2011; Bhattacharya et al., 2021) (Fig. 6).

4.4. Distribution of regular molecular markers

4.4.1. n-Alkanes

The distributions of normal alkanes in sediments and crude oils can provide detailed information about their sources of organic matter, as *n*-alkanes can originate from terrigenous higher plants, bacteria, and from

Table 2
Molecular marker parameters of Fengcheng Formation extracts from the Mahu Sag.

Sample ID	A	B	C	D	E	F	G	H	I	J	K	L	M	N
F1	0.012	0.11	0.12	0.59	0.82	0.02	1.01	7.89	0.51	0.04	0.58	0.38	0.14	0.84
F2	0.007	0.07	0.01	0.60	0.54	2.69	1.01	5.50	0.52	0.02	0.52	0.46	0.11	0.83
F3	0.003	0.03	0.04	0.60	0.41	7.82	0.79	4.06	0.50	0.07	0.46	0.46	0.05	0.95
F4	0.006	0.05	0.05	0.67	0.43	2.44	0.88	4.91	0.53	0.05	0.51	0.43	0.02	0.88
F5	0.005	0.05	0.06	0.78	0.27	0.99	0.90	4.90	0.52	0.07	0.45	0.48	0.08	0.74
F6	0.006	0.09	0.09	0.54	0.42	1.67	1.67	6.27	0.53	0.05	0.46	0.49	0.02	0.86
F7	0.001	0.01	0.01	0.76	0.31	0.74	0.28	5.01	0.55	0.09	0.46	0.45	0.02	0.80
F8	0.003	0.04	0.04	0.58	0.42	0.69	0.68	7.52	0.52	0.05	0.46	0.49	0.02	0.94

Notes: A: C_{23}–C_{25} lanostanes/C_{29}–C_{35} 17αβ hopanes; B: C_{30}–C_{32} lanostanes/C_{29}–C_{35} 17αβ hopanes; C: (C_{23}–C_{25} and C_{30}–C_{32} lanostanes)/C_{29}–C_{35} 17αβ hopanes, the lanostanes in the *m/z* 259 and the 17αβ hopanes in the *m/z* 191 of the saturated fractions; D: Pristane/Phytane; E: 7-+8-methyl heptadecanes/C_{max}; F: β-carotanes/C_{max}; G: gammacerane/ C_{30} hopanes; H: 2-MHI = 2-methyl hopanes/C_{30} hopane; I: C_{31} hopanes 22S/(22S + 22R); J: C_{27}/(C_{27}–C_{29}) regular steranes; K: C_{28}/(C_{27}–C_{29}) regular steranes; L: C_{29}/(C_{27}–C_{29}) regular steranes; M: dibenzothiophene/phenanthrene; N: MPI1.

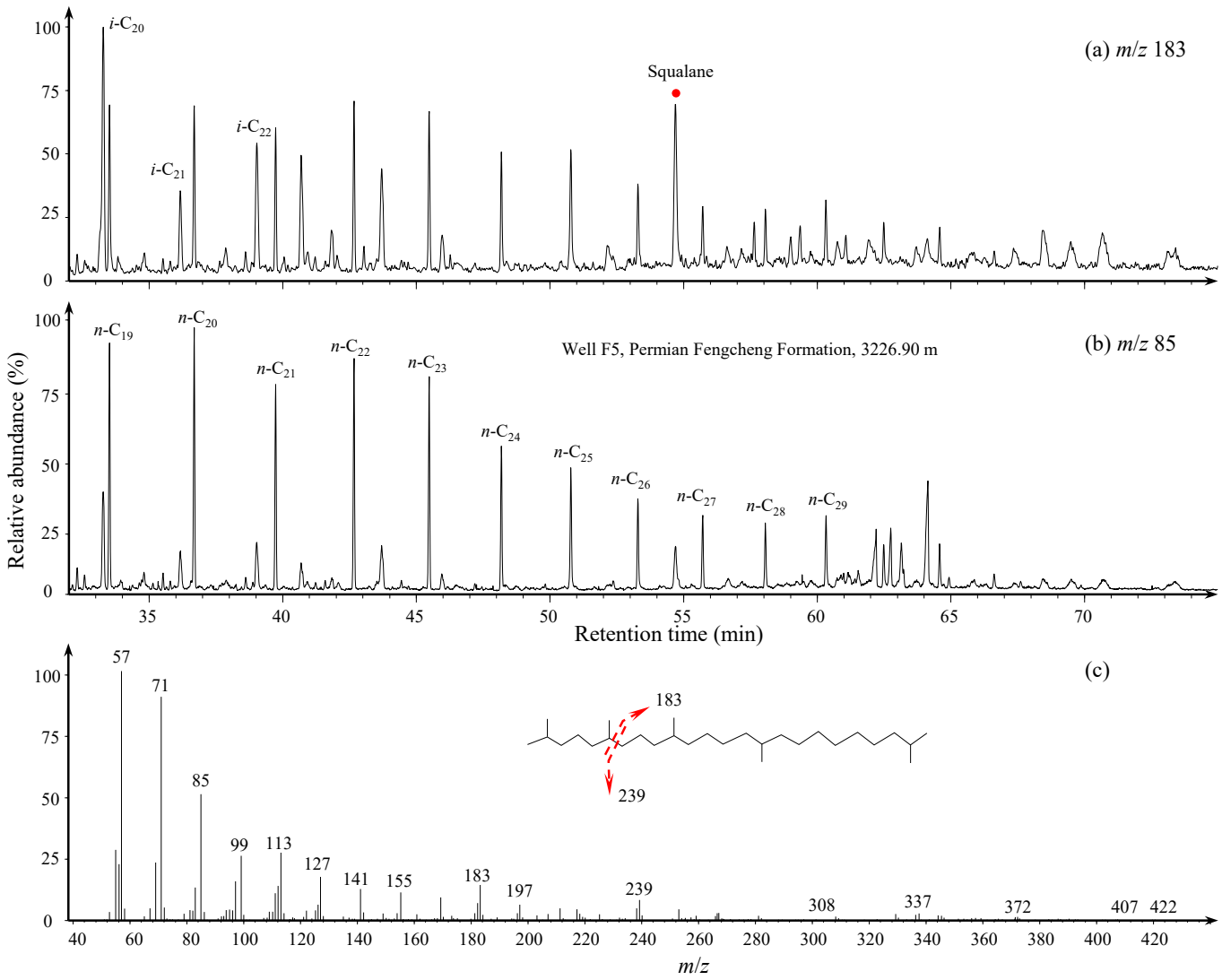

Fig. 8. Distributions of squalane and its mass spectra.

algae (Peters et al., 2005). The total ion chromatograms of saturated hydrocarbons from the source rock extracts in the study are shown in Fig. 7. The *n*-alkanes are dominated by short-chain *n*-alkanes with a unimodal mode. The carbon numbers of *n*-alkanes range from *n*-C_{14} to *n*-C_{27} with a maximum at *n*-C_{17}, suggesting a predominance of organic matter source from aquatic organisms (Brooks and Smith, 1967). A *n*-C_{17} maximum also may reflect a high maturity of source rock due to thermal cracking of long-chain alkanes. The distribution of *n*-alkanes does not show any distinct odd–even preference, suggesting that all the samples are in the oil generation window (Bray and Evans, 1961).

4.4.2. Isoprenoid alkanes

The pristane/phytane (Pr/Ph) ratio is a useful indicator for sedimentary environment determination (Brooks et al., 1969). Acyclic isoprenoids are characterized by relatively high phytane contents. The Pr/Ph ratios of source rock samples range from 0.59 to 0.78, with a mean of 0.64 (Table 2).

The mid-chain branched monomethyl and dimethyl alkanes were detected in cyanobacteria (Blumer et al., 1971; Boudou et al., 1986; Shiea et al., 1991; Köster et al., 1999), with 7- and 8-carbon substituted methyl heptadecanes predominating in modern cyanobacteria such as *Anacystis nidulans* and *Anabaena variabilis* (Blumer et al., 1971). The ratios of 7-, 8-methyl heptadecanes and C_{max} (C_{max}: predominant *n*-alkane) fall in the range 0.27–0.82 with an average of 0.45, which is unusually high.

High abundances of squalane were detected in the *m/z* 183 mass chromatograms of the saturated hydrocarbon fractions (Fig. 8a), where squalane elutes between *n*-C_{26} and *n*-C_{27} (Fig. 8b). The mass spectrum of squalane is illustrated in Fig. 8c, showing characteristic ions (*m/z* 183 and 239), and molecular ion (*m/z* 422). The relative content of squalane is higher than other isoparaffin compounds (Fig. 8a).

4.4.3. β-carotanes

Carotanes are widely detected in organic matter formed in reducing and saline water bodies (Ding et al., 2020). β-carotanes occur in the source rock extracts in this study, clearly identifiable in the total ion chromatograms of Fengcheng Formation samples (Fig. 7). The β-carotane index, β-carotane/C_{max} (where C_{max} is predominant *n*-alkane), ranges from 0.03 to 8.01 in the rock extracts (Table 2).

4.4.4. Terpanes

Hopane series, including norhopanes, hopanes, and homohopanes, were unequivocally identified in the *m/z* 191 mass chromatograms and TICs of source rock extracts (Figs. 5b, 7). The Fengcheng Formation source rocks have a particularly high gammacerane content (ten Haven et al., 1989; Sinninghe Damsté et al., 1995), with a gammacerane index ranging from 0.28 to 1.69 and averaging about 0.91 (Table 2). The C_{31} hopanes 22S/(22S + 22R) parameters of the source rocks range from

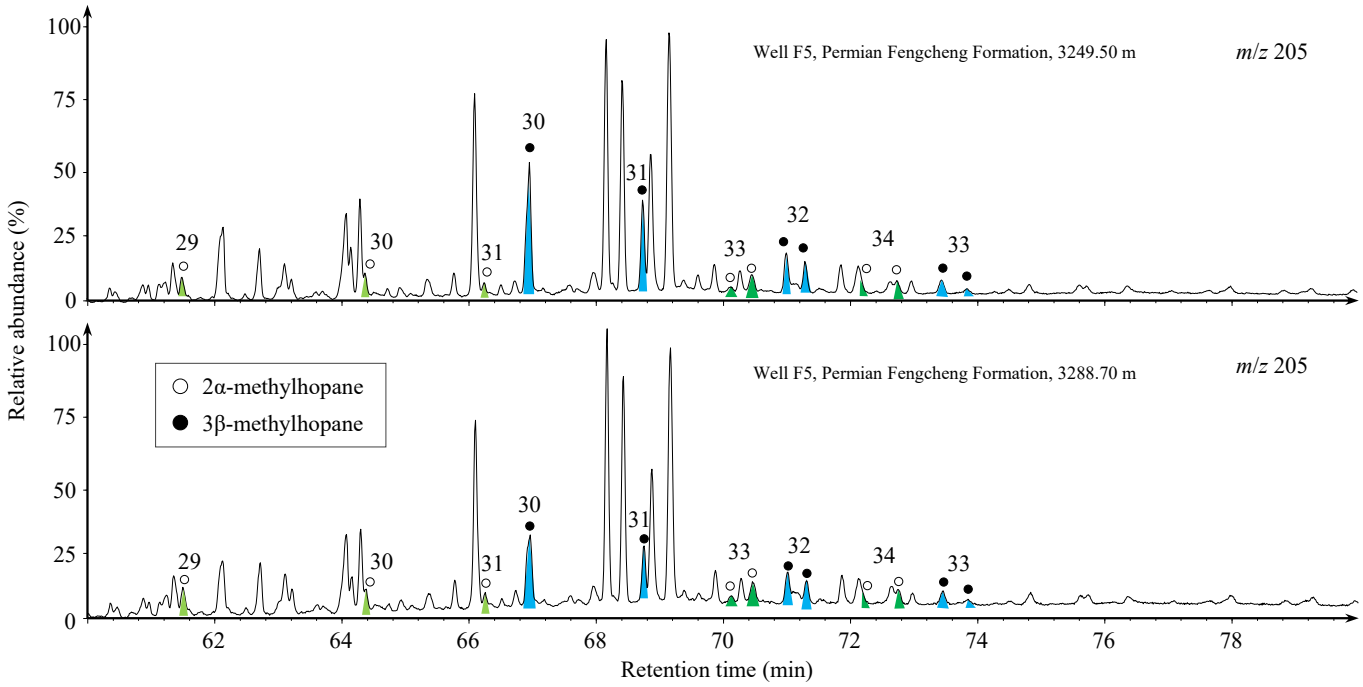

Fig. 9. Distributions of methylhopanes in the core extracts from the study area.

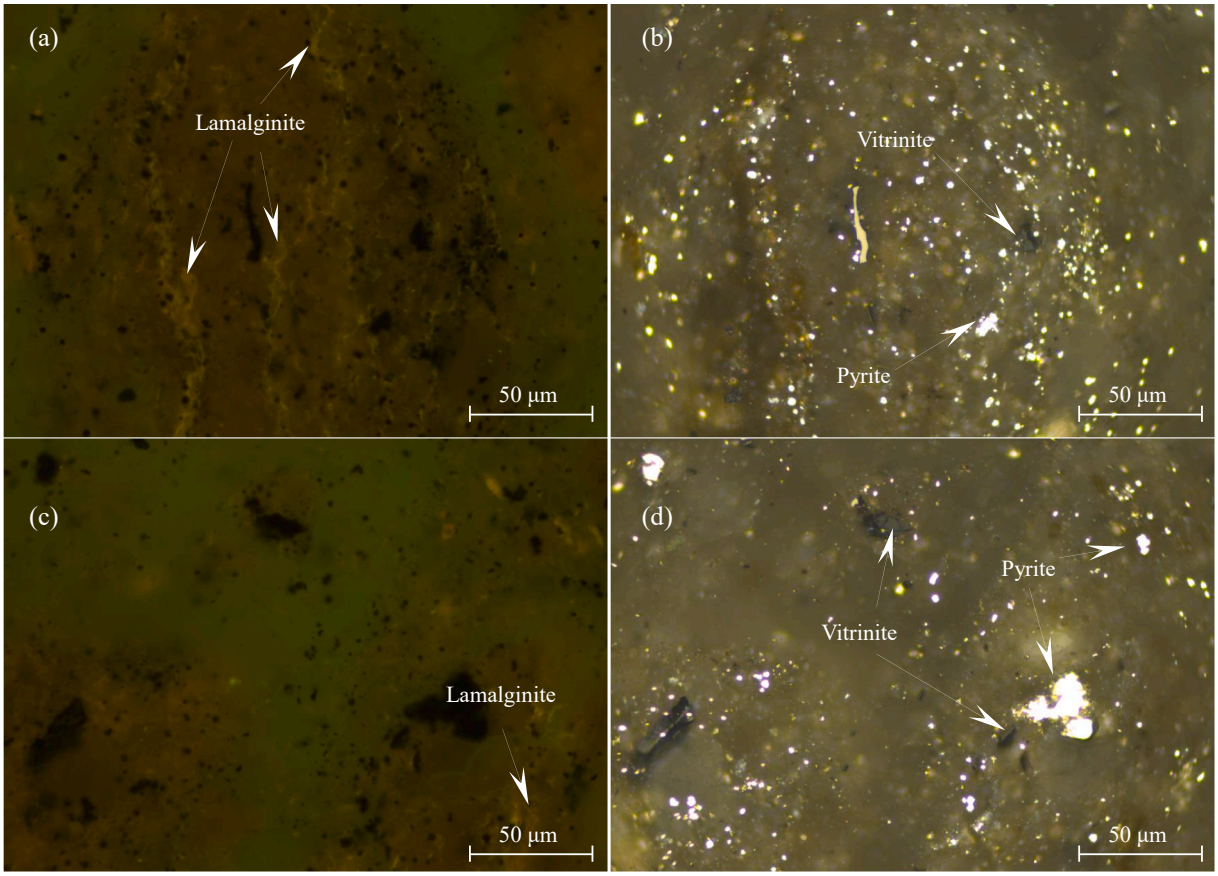

Fig. 10. Typical macerals in the core sample from well F5 with a depth of 3214.7 m.

0.50 to 0.55, where they approach or reach an equilibrium point (Zumberge, 1987) (Table 2). 2α-Methylhopanes, which are thought to be derived from cyanobacteria, occur in abundance in the samples in this work (Fig. 9) (Xie et al., 2012). The anoxygenic α-proteobacteria also may be main precursors for the compounds (Welander et al., 2010; Naafs et al., 2022). The 2α-methylhopanes/C_{30} hopane ratio ranges from

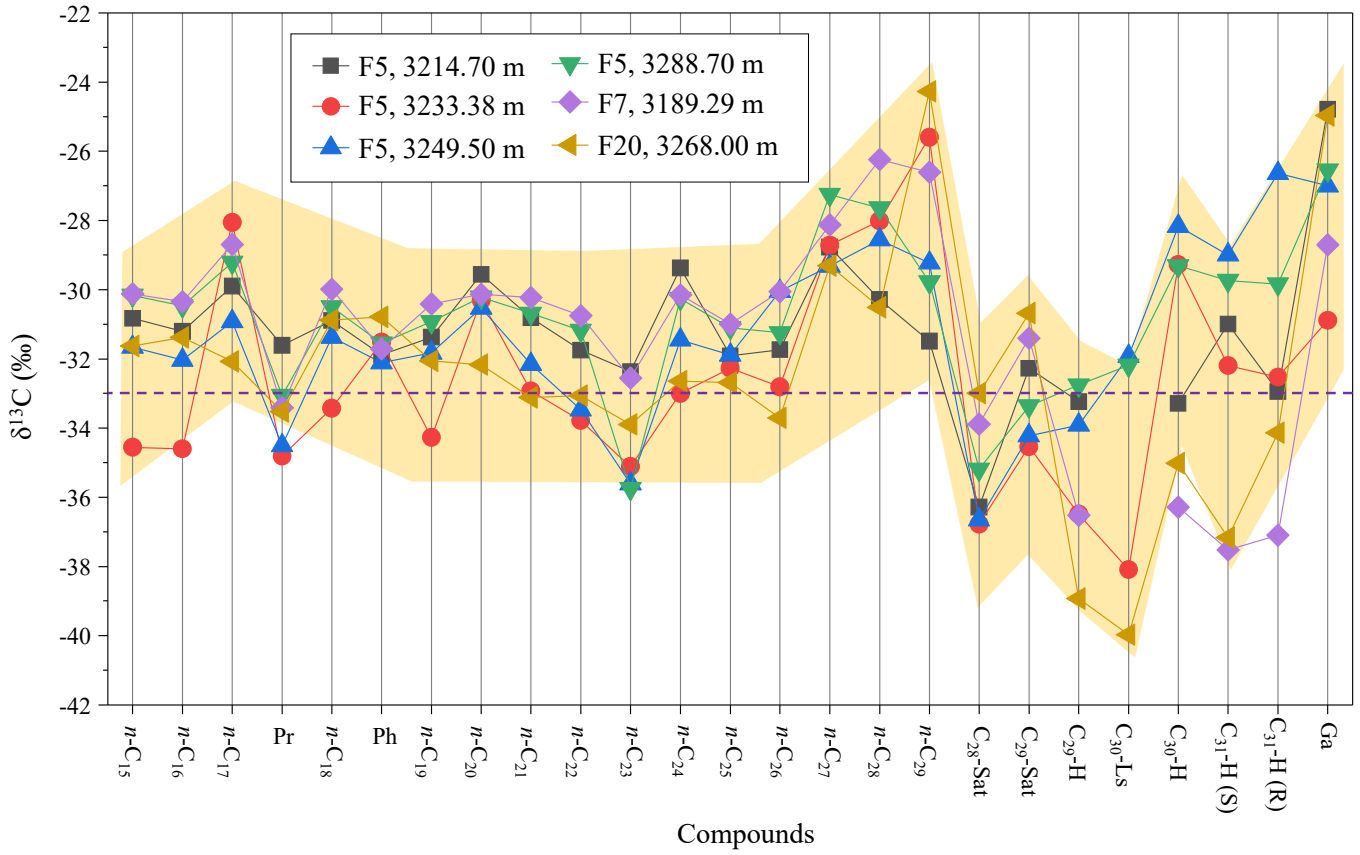

Fig. 11. Compound specific stable carbon isotope composition in the studied samples. Pr, pristane; Ph, phytane; C_{28}-Sat, C_{28} ααα 20R regular sterane; C_{29}-Sat, C_{29} ααα 20R regular sterane; C_{29}-H, C_{29} αβ hopane; C_{30}-Ls, C_{30} lanostane; C_{30}-H, C_{30} αβ hopane; C_{31}-H (S), C_{31} αβ 22S hopane; C_{31}-H (R), C_{31} αβ 22R hopane; Ga, gammacerane.

Table 3
The stable carbon isotope composition of individual compounds.

Compounds/Sample ID	F1 ($\delta^{13}C$, ‰)	F3 ($\delta^{13}C$, ‰)	F4 ($\delta^{13}C$, ‰)	F5 ($\delta^{13}C$, ‰)	F7 ($\delta^{13}C$, ‰)	F8 ($\delta^{13}C$, ‰)
n-C_{15}	−30.8	−34.6	−31.7	−30.2	−30.1	−31.6
n-C_{16}	−31.2	−34.6	−32.0	−30.5	−30.3	−31.4
n-C_{17}	−29.9	−28.1	−30.9	−29.2	−28.7	−32.1
Pristane	−31.6	−34.8	−34.5	−33.1	−33.4	−33.5
7-+8-methylheptadecan	−30.8	−30.6	−31.4	−30.4	−38.2	−28.8
n-C_{18}	−30.9	−33.4	−31.4	−30.5	−30.0	−30.9
Phytane	−31.9	−31.5	−32.1	−31.5	−31.7	−30.8
n-C_{19}	−31.4	−34.3	−31.8	−30.9	−30.4	−32.1
n-C_{20}	−29.6	−30.3	−30.5	−30.2	−30.1	−32.2
n-C_{21}	−30.8	−32.9	−32.2	−30.7	−30.2	−33.1
n-C_{22}	−31.7	−33.8	−33.5	−31.2	−30.8	−33.1
n-C_{23}	−32.4	−35.1	−35.6	−35.8	−32.6	−33.9
n-C_{24}	−29.4	−33.0	−31.5	−30.3	−30.2	−32.6
n-C_{25}	−31.9	−32.3	−31.9	−31.1	−31.0	−32.7
n-C_{26}	−31.7	−32.8	−30.0	−31.2	−30.1	−33.7
n-C_{27}	−28.8	−28.7	−29.3	−27.3	−28.1	−29.3
n-C_{28}	−30.3	−28.0	−28.6	−27.6	−26.2	−30.5
n-C_{29}	−31.5	−25.6	−29.2	−29.8	−26.6	−24.3
C_{28}-Sterane (Sat)	−36.3	−36.8	−36.7	−35.2	−33.9	−33.0
C_{29}-Sterane (Sat)	−32.3	−34.5	−34.2	−33.4	−31.4	−30.7
C_{29}-Hopane (H)	−33.2	−36.5	−33.9	−32.8	−36.5	−38.9
C_{30}-Lanostane (Ls)	nd	−38.1	−31.9	−32.2	nd	−40.0
C_{30}-Hopane (H)	−33.3	−29.3	−28.2	−29.3	−36.3	−35.0
C_{31}-Hopane (H) S	−31.0	−32.2	−29.0	−29.7	−37.5	−37.2
C_{31}-Hopane (H) R	−32.9	−32.5	−26.6	−29.8	−37.1	−34.1
Gammacerane	−24.8	−30.9	−27.0	−26.5	−28.7	−25.0

Note: nd: no data.

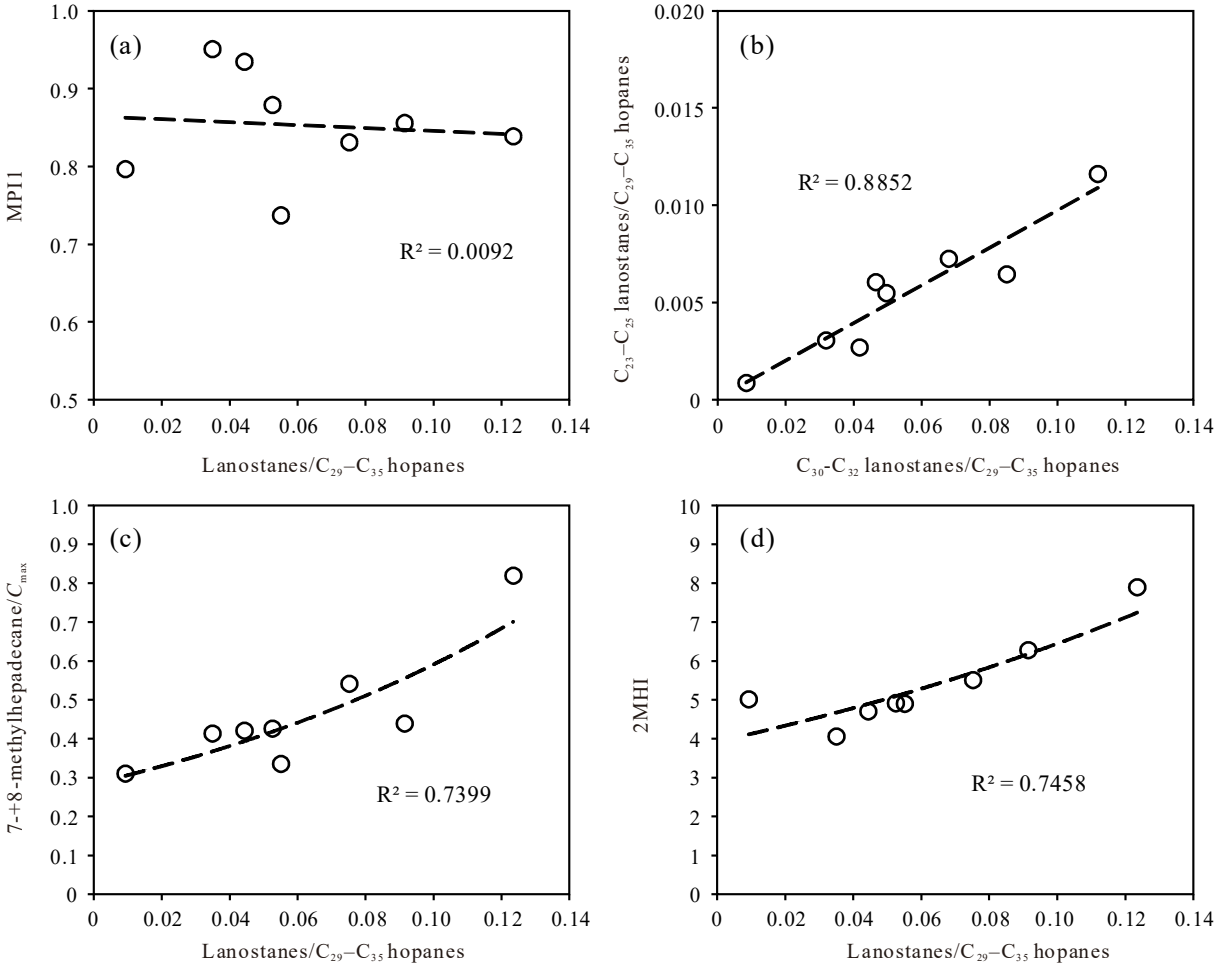

Fig. 12. Cross plots of (a) the relative abundance of lanostanes vs methylphenanthrene index, MPI1 = 1.5(2-MP + 3-MP)/(P + 1-MP + 9-MP), (b) the relative abundance of C_{30}–C_{32} lanostanes vs C_{23}–C_{25} lanostanes, (c) the relative abundance of lanostanes vs 7-+8-methyl hepadecane/C_{max}, C_{max}: predominant *n*-alkane in total ion current; (d) the relative abundance of lanostanes vs 2-methyl hopanes index, 2-MHI = C_{31} 2-methylhopanes/(C_{31} 2-methylhopanes + C_{30} hopane).

4.06 to 7.89 (average 5.76) (Table 2).

4.4.5. Steroids

Sterane series are characterized by high content of C_{27}–C_{29} regular steranes (Figs. 2c, 7). The C_{28} and C_{29} steranes are dominated with relative proportions of C_{28} and C_{29} steranes are 0.46–0.58 and 0.38–0.49, respectively, while the C_{27} steranes are in lower proportions of 0.02–0.09 (average 0.05) (Table 2).

C_{28}–C_{30} and C_{22}–C_{24} 4-methyl steranes also were observed in the extracts dominated by longer chain species (Fig. 2d). A series of 4,4-dimethylsteranes (C_{29}–C_{31}, C_{23}–C_{25}) were present with a base peak at *m/z* 245 (Fig. 2e), and the long-chain species are relatively abundant.

4.5. Maceral composition

The macerals of Fengcheng Formation source rock mainly consist of lamalginite, vitrinite and pyrite (Fig. 10). Lamalginite, with a yellowish fluorescence, is abundant (Fig. 10a, c), while the relative abundance of vitrinite is lower (Fig. 10b, d). The cores have a large amount of internal pyrite framboids, characterized by a strong reflection and non-fluorescence (Fig. 10) that indicate the bacterial sulfate reduction during deposition.

4.6. Isotope compositions of individual biomarker

Fig. 11 shows the stable carbon isotope ($\delta^{13}C$) composition of individual compound including *n*-alkanes, hopanes, regular steranes and lanostane. The $\delta^{13}C$ values of *n*-alkanes range from −35.8 ‰ to −24.3 ‰ (Table 3). The isotope composition of *n*-alkanes with high carbon number (*n*-C_{27}–*n*-C_{29}) is distinctly more enriched than the *n*-alkanes with low carbon number (*n*-C_{15}–*n*-C_{26}), which may indicate a different biological source. The $\delta^{13}C$ values of pristane and phytane are within the range of −34.8 ‰ to −31.6 ‰ and −32.1 ‰ to −30.8 ‰, respectively. The $\delta^{13}C$ values of C_{28} ααα 20S regular sterane (−36.8 ‰ to −33.0 ‰) are lower than those of C_{29} 20S ααα regular sterane (−34.5 ‰ to −30.7 ‰). The C_{30}- and C_{31}-hopanes are ^{13}C enrich compared to C_{29} hopane. The $\delta^{13}C$ values of gammacerane range in −24.8 ‰ to −30.9 ‰.

5. Discussion

5.1. Effect of maturity on the concentrations of lanostanes

Maturity of organic matter has an important influence on the concentrations of biomarkers. Generally, the concentrations of molecular biomarkers in sediments and crude oils decrease with increasing maturity (Peters et al., 2005). The Fengcheng Formation samples in this study are mature–high mature as implied by vitrinite reflectance (%Ro), C_{31} hopanes 22S/(22S + 22R) and methylphenanthrene index (MPI) (Radke, 1983) (Table 2). Lanostanes are abundant in the high-mature Fengcheng Formation samples (Fig. 12), which shows that the thermal maturity has only a minor influence on them. There is also a very poor correlation between the concentration of lanostanes and MPI1, which

again demonstrates that abundance of lanostanes is not affected by maturity (Fig. 12a). The short-chain lanostanes may be yielded from long-chain compounds by side-chain cleavage occurring at high maturity. However, the relative abundances of short-chain lanostanes have a minor change with MPI1 (Table 2) may due to a narrow range of MPI1. So the relationship between those compounds and maturity remains to be seen.

5.2. Origin of lanostanes

The relative abundance of C_{23}–C_{25} and C_{30}–C_{32} lanostanes correlate shows a significant positive correlation between short-chain and long-chain lanostanes, strongly suggesting a similar origin for the two series (Fig. 12b).

Lanostanes are believed to be derived from lanosterols (Chen et al., 1989). However, the origin of lanosterols remains a controversial issue, because they occur widely in terrigenous higher plants, bacteria and algae (Summons et al., 2006). However, the distributions of *n*-alkanes, acyclic isoprene, and hopane series (Figs. 5, 7) and maceral compositions (Fig. 10) in the Fengcheng Formation source rocks imply that the organic matter source comes from aquatic organisms. Terrigenous higher plants have made little contribution to the lanosterols in Fengcheng Formation.

7- and 8- Methylalkanes are considered to be highly specific for cyanobacteria (Blumer et al., 1971; Dobson et al., 1988; Shiea et al., 1990; Kenig et al., 1995; Luo et al., 2015). The relative contents of 7- and 8- monomethyl-substituted heptadecanes are distinctly higher than those of other isomers in the Fengcheng Formation extracts (Fig. 7). The relative concentrations of lanostanes and 7- and 8- methyl heptadecane/C_{max} (C_{max}: predominant *n*-alkane) shows that the abundance of lanostanes increases with the relative content of 7- and 8- methyl heptadecane (Fig. 12c), suggesting that the lanostanes might also derived from cyanobacteria.

The origin of 2α-methylhopane is not clear. It is generally considered to be derived from cyanobacteria (Summons et al., 1999; Xie et al., 2005; Eigenbrode et al., 2008). However, Hoshino et al., (2023) suggested that hopanoid C-2 methyltransferase occurred in *Alphaproteobacteria* using genetics and showed that proteobacterial sources appear to dominate in the Phanerozoic. 2α-Methylhopane was observed in the core extracts from the study area (Fig. 9). The relative abundance of 2α-methylhopane appears to be lower than those of 3β-methylhopane, which may be related to the alkaline environment. It is reported that the relatively enhanced 3β-methylhopanes usually occur in modern and ancient alkaline sediments, e.g. Green River Formation (Farrimond et al., 2004), and sedimentary rocks deposited in saline environment, e.g. Permian Lucaogou Formation the Junggar Basin (Ding et al., 2020). Colloster et al. (1991) suggested that αβ-hopanes and 3β-methylhopanes show a significant depletion in ^{13}C in the Green River shale due to a major contribution from methanogens. Previous investigators showed that the isotope compositions of hopanes biosynthesized by cyanobacteria are significantly enriched in ^{13}C (4.5 ‰–9.0 ‰) (Hayes, 1990; Sakata et al., 1997; Summons et al., 1998). The $\delta^{13}C$ values of αβ-hopane are between −28.2 ‰ and −37.5 ‰ with an average of −33.0 ‰ may indicate a cyanobacterial source (Table 3). Based on the biomarker, fossils and microbial community structure analysis, Hou et al. (2022) suggested that cyanobacteria were the major organic input for the Fengcheng Formation strata deposited in an alkaline lake. Therefore, we conclude that the abundance of 2α-methylhopanes may reflect a significant contribution of cyanobacteria in organic matter of Fengcheng Formation in the study area. The relative content of lanostanes has a strong correlation with the 2-methyl hopanes index (2-MHI = 2-methyl hopanes/C_{30} hopane) (Fig. 12d), suggesting common biological precursors.

Generally, a predominance of C_{27} sterane components is associated with input from aquatic organisms, while C_{28} and C_{29} steranes are mainly derived from terrigenous higher plants (Huang and Meinschein, 1979). However, high contents of C_{28} and C_{29} regular steranes have been detected in numerous studies of sediments in different basins with input from algal organic matter (Cai et al., 2009; Wan et al., 2014; Liu et al., 2022). Liu et al. (2022) proposed, based on organic petrology, that cyanobacteria may be the primary source of the abundant C_{28} regular steranes found in the Permian Lucaogou Formation in the Junggar Basin. The C_{29} regular steranes may be also sourced form cyanobacteria (Mckirdy and Hahn, 1982; Fowler and Douglas, 1987). Hou et al. (2022) attributed the abundant C_{29} steranes in the Fengcheng Formation to the cyanobacteria input. Organic petrology also supports the position that abundant cyanobacteria in Fengcheng Formation source rocks are main source of organic matter in the Mahu Sag (Hou et al., 2022; Xia et al., 2022). The alginates include telalginite and lamalginite. Telalginite generally refers to green algae occurred with diverse forms. The dinoflagellates, coccolithophores, diatoms, and brown algae became prevailing after the Triassic. A low abundance of telalginite are present in the studied samples likely because of the heterogeneity of the sediments. Lamalginite is considered to be generated from algal and/or cyanobacterial remains (Peniguel et al., 1989). The high abundances of lamalginite may be attributing to the cyanobacterial and algal source (Fig. 11). The Fengcheng Formation extracts are characterized by high contents of C_{28} and C_{29} regular steranes (Fig. 2c, 7). Carbon isotopic compositions of C_{28} and C_{29} steranes −36.8 ‰ to −30.7 ‰ suggest these compounds may be derived from chemoautotrophic bacteria growing near the lake surface. Hence, it is concluded that the dominance of C_{28} and C_{29} regular steranes in all the Fengcheng Formation samples may be attributed to the contribution of cyanobacteria to the organic matter in the formation. Co-occurrence of abundant C_{28} and C_{29} regular steranes and lanostanes indicates that cyanobacteria are likely to be their common biological source.

Although sterol biosynthesis in cyanobacteria has been reported, Summons et al. (2006) showed evidence for sterol biosynthesis by cyanobacteria appears flawed because cyanobacterial cultures are easily contaminated by sterol-producing rust fungi, which can be eliminated by treatment with cycloheximide affording sterol-free samples. Xia et al. (2022) also showed that the organic matter source of Fengcheng Formation deposited in the central of the ancient alkaline lake are mainly *Dunaliella*-like algae and those in the margin of the alkaline lake (e.g. well F5 studied in this work) are mainly cyanobacteria. The contributions of algae and cyanobacteria for Fengcheng Formation may be very heterogeneous. However, the samples from the central region are not included in this study. Therefore, the relationship between lanosterol and cyanobacteria need further studied.

Compound specific isotopic analyses of phytane (−32.1 ‰ to −30.8 ‰) (Table 3, Fig. 12) from these core samples are consistent with input from primary photosynthetic producers such as cyanobacteria (Ruble et al., 1994). The isotope values of 7-+8-methyl heptadecane (average −31.7 ‰) (Table 3) are similar with those of phytane which may indicate a common source for these compounds. The similarity of isotopic compositions for C_{28} regular steranes and C_{30} lanostane also may suggest a common biological source of those molecular markers sharing a similar environment, i.e. the photic zone of ancient alkaline lake during Fengcheng Formation deposition. The $\delta^{13}C$ values of αβ-hopane range from −28.2 ‰ to −37.5 ‰ with a mean of −33.0 ‰ (Table 3, Fig. 11). Numerous authors have reported that extreme depletions in ^{13}C for hopanes, 3β-methylhopanes and lanostanes ($\delta^{13}C$ = ~−70 ‰) and suggested these compounds may be derived from methanotrophic organisms (e.g. Colloster et al., 1991; Ruble et al., 1994; Brigel and Peckmann, 2008). Compared with isotope compositions of hopanes in the previous reports, the hopanes are significantly enriched in ^{13}C and may be due to the distinct dominance of other organisms e.g. cyanobacteria or sulfate-reducing bacteria in the alkaline lacustrine environment. The isotope compositions of C_{30} lanostane is similar to those of steranes and hopanes consistent with their common sources. The contributions of algae for the organic matter of the Fengcheng Formation also should be considered because of the similar compound specific

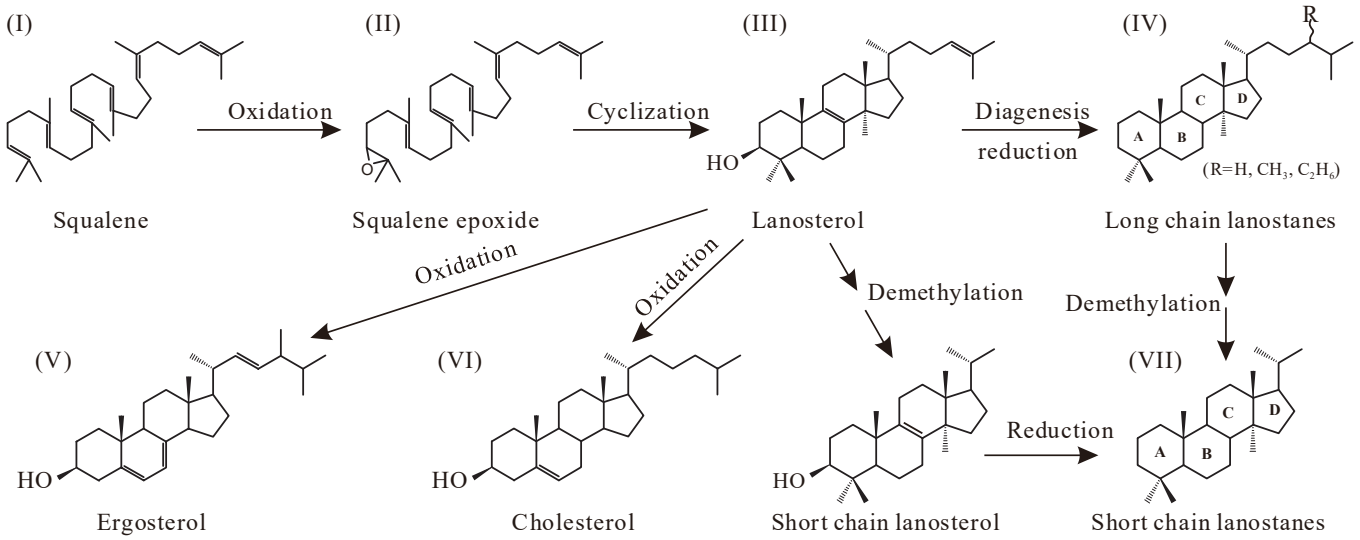

Fig. 13. Proposed conceptual biosynthetic reaction schemes for the formation of short chain lanostanes (modified from Summons et al. (1985); Chen et al. (1989)).

isotope components and should be investigated using more geological samples considering the heterogeneity.

In summary, based on the maceral characteristics and isotopic compositions, the 7-+8-methyl heptadecanes, 2α-methyl hopanes and C_{28} and C_{29} steranes may be derived from phototrophs (cyanobacteria) in the Fengcheng Formation from the Mahu Sag although the attribution of steranes to cyanobacteria is recognized as controversial.

5.3. Identifying the sedimentary

In general, Pr/Ph ratios less than 0.8 imply strongly reducing conditions, while Pr/Ph ratios greater than 3 indicate distinctly oxidic water bodies (Didyk et al., 1978; ten Haven et al., 1988). The Pr/Ph values of the Fengcheng Formation extracts are very low (Table 2), suggesting a reducing environment during deposition of the formation. High concentrations of β-carotanes also indicate a strongly reducing environment (Murphy et al., 1967; Requejo et al., 1992; Hopmans et al., 2005; Ding et al., 2020). Gammacerane content reflects the salinity of the water body (Philp and Fan, 1987; ten Haven et al., 1989; Sinninghe Damsté et al., 1995). The Fengcheng Formation extracts are characterized by high concentrations of gammacerane (Table 2), indicating that the organic matter in the Fengcheng Formation source rocks formed with a hypersaline water body. In addition, abundant alkaline minerals, such as wegscheiderite, trona (Yu et al., 2018), reedmergnerite (Guo et al., 2021), searlesite, and chert (Yu et al., 2021), are found in Fengcheng Formation, which are diagnostic of an alkaline environment. In summary, the combined geochemical and sedimentological evidence strongly favors the view that the lanostanes in the Fengcheng Formation source rock are associated with a strongly reducing, hypersaline environment.

5.4. Possible formation pathways

Chen et al. (1989) proposed that C_{30} lanostane in sediments forms from biological lanosterol via reductive diagenetic reactions. As illustrated in Fig. 13, one possible reaction pathway is that oxidation of squalene (I) can biosynthetically produce squalene epoxide (II) (Summons et al., 2006), which is then transformed to lanosterols (III) via cyclization. Finally, the lanosterols can generate saturated compounds, i.e. lanostanes (IV) via hydrogenation reactions during diagenesis phase in a hypersaline environment (Bhattacharya et al., 2021). Another possible pathway is that lanosterols (III) can be converted into cholesterols (VI) (C_{27}–C_{29}), which finally transform into C_{27}–C_{29} steranes. Demethylation of long chain lanostanes (IV) can create short-chain lanostanes (VII). Lu et al. (2011) suggested that C_{24} and C_{25} lanostanes can be formed by cleavage of weak C–S bonds at the C22 position of sulfur containing steroids, which has been confirmed to contain a sulfur linkage (Peng et al., 1998; Lu et al., 2011). However, although this mechanism may explain the formation of short-chain lanostanes in sulfur-rich oils and sediments, it does not apply to the sulfur-poor lacustrine sediments in this study (Cao et al., 2020).

5.5. Accumulation model of the lanostanes

The preservation of volcanic rocks intercalated within mudstones in the northeast margin of the Mahu Sag were interpreted to be influenced by volcanism in the northern part of lake (Wang et al., 2021c). This volcanism prevailed during the deposition of the Fengcheng Formation, due to violent tectonic movement during the Carboniferous-Early Permian in the northwestern margin of Junggar Basin (Li et al., 2020; Wang et al., 2021b). The volcanic glass and volcanic ash contain abundant magnesium- and iron-rich materials (Duggen et al., 2007). When iron is ample, H_2S can easily sequestered as Fe-sulfide (such as pyrite) (Fig. 8b, d) before it can react with organic matter leading to less abundant organic sulfur compounds including dibenzothiophene (DBT) (Werne et al., 2008; Asif et al., 2009). The ratio of dibenzothiophene to phenanthrene (DBT/P) is related with the concentration of sulfate under reducing conditions (Werne et al., 2008; Luo et al., 2019). DBT/P values of the Fengcheng Formation sediments in the Mahu Sag are very low, ranging from 0.02 to 0.08 (average 0.05) (Table 2), which indicates a low sulfate content during deposition of the organic matter. The high abundance of β-carotane in the Fengcheng Formation sediments is also consistent with an environment with low sulfate concentration (Ding et al., 2020).

The lake level of the Mahu Sag was overall lower due to the high evaporation during the deposition of the Fengcheng Formation and the presumed depth of the water body may be 0–80 m based on the sedimentary facies (shoreline-shallow lake and semi-deep lake) of the strata (Wang et al., 2021b), which is suitable for the living of the photosynthetic organisms. Abundant laminated stromatolites and *Chroococcus* fossil (a cyanobacteria species) have been observed in the cores from the Fengcheng Formation (Hou et al., 2022). Yu et al. (2021) showed that the banded chert bear the large amount of spheroidal cyanobacteria cells that can be attributed to the chemical precipitate with the aid of those microorganism. These bedded sediments may be a record of algal or cyanobacterial mats. The magnesium and iron brought by the volcanic

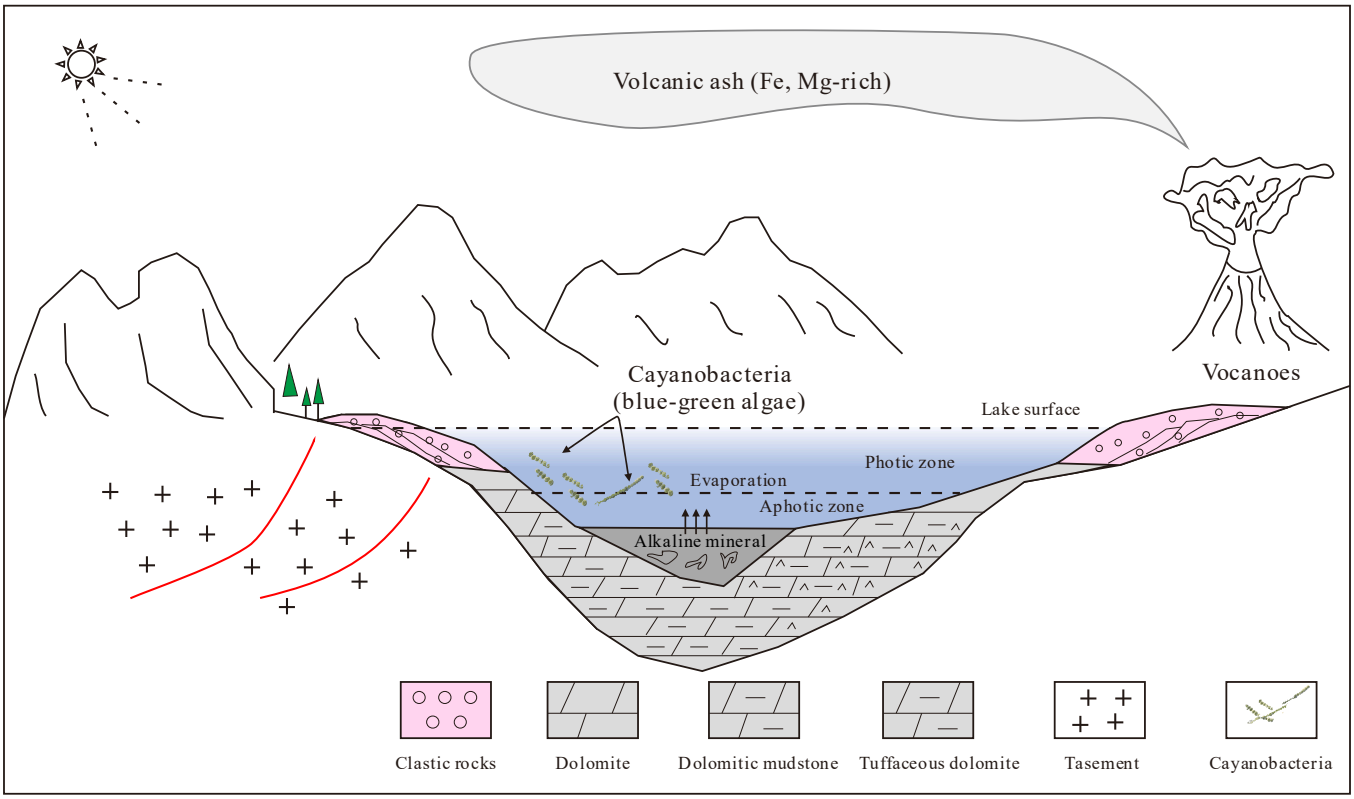

Fig. 14. Accumulation model of the lanostanes in the Fengcheng Formation of the Mahu Sag, Junggar Basin.

ash can fertilize the cyanobacteria and algae having the squalene epoxide biosynthesis process, which may result in the lanostanes accumulation in the Fengcheng Formation of the Mahu Sag. The saline environment of the stratified water body is helpful for the preservation of cyanobacteria and algae (Brocks et al., 2003; Talbot et al., 2008).

Hypersaline lacustrine and marine environments with carbonate and evaporite precipitation are known to favor the growth of cyanobacteria mats (e.g., Des Marais, 2003; Wieland et al., 2008). Many alkaline and carbonate minerals are present in the Fengcheng Formation, indicating a hypersaline water body during deposition (Yu et al., 2018, 2021). As discussed above, the primary precursors of lanostanes in the Fengcheng Formation may be cyanobacteria, which are more abundant in the evaporitic and carbonate-rich sediments (Ding et al., 2020). In the saline water environment with hydrologic closure of the Fengcheng Formation, waters with terrigenous clastic sediments input are appropriate to boost photosynthetic microbial mats (Fig. 14).

6. Conclusions

A series of short-chain lanostanes, including a tentatively identified C_{23} homologue, was detected in dolomitic mudstone from the Lower Permian Fengcheng Formation in the Mahu Sag, Junggar Basin. Co-occurrence of both long and short-chain lanostanes, and the positive correlations between their relative content suggest a common biological source. The effect of maturity on the relative abundance of short-chain lanostanes is minor, although this is likely due to a narrow range of maturity of the studied samples. Lamalginite (thin-walled colonial or unicellular algae that includes cyanobacteria) is abundant in the cores. Carbon isotopic compositions of individual compounds (hopanes, steranes and C_{30} lanostane) are similar, suggesting these compounds were derived from a common source inferred to be primary producers (including cyanobacteria) from the oxygenated photic. It is tentatively speculated that cyanobacteria may be a biological source of lanostanes in Fengcheng Formation organic matter because of the occurrence along with abundant 7-+8-methyl heptadecane and 2-methylhopanes. However, occurrence of high abundances of C_{28} and C_{29} steranes and β-carotane indicate that algal sources for these compounds also need be considered. The satisfactory explanations are limited by the absence of Fengcheng Formation samples deposited in the ancient central region. The abundance of short-chain lanostanes in a typical alkaline lake shows that they are potential molecule biomarkers for paleoenvironment interpretation and oil-source rock correlation.

Declaration of competing interest

The authors declare that they have no known competing financial interests or personal relationships that could have appeared to influence the work reported in this paper.

Data availability

Data will be made available on request.

Acknowledgements

This work is supported by the National Natural Science Foundation of China (Grant No. 42202134). The authors thank the Research Institute of Experiment and Detection, Xinjiang Oilfield Company, CNPC for providing samples and permission to publish. We would like to express our gratitude to Dr. Clifford C. Walters, Dr. John Volkman and two anonymous reviewers for their constructive suggestions. Thanks are due to Shengbao Shi, Lei Zhu, Tiantian Li and Shuofan Li for their generous assistance with the experiments.

References

Asif, M., Alexander, R., Fazeelat, T., Pierce, K., 2009. Geosynthesis of dibenzothiophene and alkyl dibenzothiophenes in crude oils and sediments by carbon catalysis. Organic Geochemistry 40, 895–901.

Bechtel, A., Movsumova, U., Pross, J., Gratzer, R., Ćorić, S., Sachsenhofer, R.F., 2014. The Oligocene Maikop series of Lahich (eastern Azerbaijan): paleoenvironment and oil–source rock correlation. Organic Geochemistry 71, 43–59.
Bhattacharya, S., Dutta, S., Kumar, S., 2021. Identification of lanostanes, A-ring methylated steranes and secosteranes in late Neoproterozoic crude oils by GC×GC-TOFMS: new insights into molecular taphonomy of steroids. Geobios 68, 47–59.
Blumer, M., Guillard, R.R.L., Chase, T., 1971. Hydrocarbons of marine phytoplankton. Marine Biology 8, 183–189.
Boudou, J.P., Trichet, J., Robinson, N., Brassell, S.C., 1986. Profile of aliphatic hydrocarbons in a recent Polynesian microbial mat. International Journal of Environmental Analytical Chemistry 26, 137–155.
Bray, E.E., Evans, E.D., 1961. Distribution of *n*-paraffins as a clue to recognition of source beds. Geochimica et Cosmochimica Acta 22, 2–15.
Brigel, D., Peckmann, J., 2008. Aerobic methanotrophy at ancient marine methane seeps: a synthesis. Organic Geochemistry 39, 1659–1667.
Brocks, J.J., Buick, R., Summons, R.E., Logan, G.A., 2003. A reconstruction of Archean biological diversity based on molecular fossils from the 2.78 to 2.45 billion-year-old Mount Bruce Supergroup, Hamersley Basin, Western Australia. Geochimica et Cosmochimica Acta 67, 4321–4335.
Brooks, J.D., Smith, J.W., 1967. The diagenesis of plant lipids during the formation of coal, petroleum and natural gas—I. Changes in the *n*-paraffin hydrocarbons. Geochimica et Cosmochimica Acta 31, 2389–2397.
Brooks, J.D., Gould, K., Smith, J.W., 1969. Isoprenoid hydrocarbons in coal and petroleum. Nature 222, 257–259.
Cai, C., Li, K., Anlai, M., Zhang, C., Xu, Z., Worden, R.H., Wu, G., Zhang, B., Chen, L., 2009. Distinguishing Cambrian from Upper Ordovician source rocks: evidence from sulfur isotopes and biomarkers in the Tarim Basin. Organic Geochemistry 40, 755–768.
Cao, J., Xia, L., Wang, T., Zhi, D., Tang, Y., Li, W., 2020. An alkaline lake in the Late Paleozoic Ice Age (LPIA): a review and new insights into paleoenvironment and petroleum geology. Earth-Science Reviews 202, 103091.
Chen, J., Fu, J., Sheng, G., Philp, R.P., Ma, W., 1990. A novel series of tetracyclic triterpenoid hydrocarbons: lanostanes (C_{30}–C_{32}). Science China-Chemistry 6, 632–638.
Chen, J.H., Philp, R.P., Fu, J.M., Sheng, G.Y., 1989. The occurrence and identification of C_{30}–C_{32} lanostanes: a novel series of tetracyclic triterpenoid hydrocarbons. Geochim. Geochimica et Cosmochimica Acta 53, 2775–2779.
Chen, J., Summons, R.E., 2001. Complex patterns of steroidal biomarkers in Tertiary lacustrine sediments of the Biyang Basin, China. Organic Geochemistry 32, 115–126.
Colloster, J.M., Summons, R.E., Lichtfouse, E., Hayes, J.M., 1991. An isotope biogeochemical study of the Green River oil shale. Organic Geochemistry 1991, 265–276.
Des Marais, D., 2003. Biogeochemistry of hypersaline microbial mats illustrates the dynamics of modern microbial ecosystems and the early evolution of the biosphere. Biological Bulletin 204, 160–167.
Didyk, B.M., Simoneit, B.R.T., Brassell, S.C., Eglinton, G., 1978. Organic geochemical indicators of palaeoenvironmental conditions of sedimentation. Nature 272, 216–222.
Ding, W., Hou, D., Jiang, L., Jiang, Y., Wu, P., 2020. High abundance of carotanes in the brackish-saline lacustrine sediments: a possible cyanobacteria source? International Journal of Coal Geology 219, 103373.
Dobson, G., Ward, D.M., Robinson, N., Eglinton, G., 1988. Biogeochemistry of hot spring environments: extractable lipids of a cyanobacterial mat. Chemical Geology 68, 155–179.
Duggen, S., Croot, P., Schacht, U., Hoffmann, L., 2007. Subduction zone volcanic ash can fertilize the surface ocean and stimulate phytoplankton growth: evidence from biogeochemical experiments and satellite data. Geophysical Research Letters 34, 1–5.
Eigenbrode, J.L., Freeman, K.H., Summons, R.E., 2008. Methylhopane biomarker hydrocarbons in Hamersley Province sediments provide evidence for Neoarchean aerobiosis. Earth and Planetary Science Letters 273, 323–331.
Espitalié, J., Deroo, G., Marquis, F., 1985. La pyrolyse Rock-Eval et ses applications. Deuxième partie. Revue de l'Institut Français du Pétrole 40, 755–784.
Farrimond, P., Talbot, H.M., Watson, D.F., Schulz, L.K., Wilhelms, A., 2004. Methylhopanoids: molecular indicators of ancient bacteria and a petroleum correlation tool. Geochimica et Cosmochimica Acta 68, 3873–3882.
Fowler, M.G., Douglas, A.G., 1987. Saturated hydrocarbon biomarkers in oils of Late Precambrian age from Eastern Siberia. Organic Geochemistry 11, 201–213.
Guo, P., Wen, H., Li, C., Jin, J., Lei, H., 2021. Origin and enrichment of borates in a Late Paleozoic alkaline lake-playa deposit, Junggar Basin, NW China. Ore Geology Reviews 138, 104389.
Hayes, J.M., 1990. Compound-specific isotopic analyses: a novel tool for reconstruction of ancient biogeochemical processes. Organic Geochemistry 16, 1115–1128.
Hopmans, E.C., Schouten, S., Rijpstra, W.I.C., Sinninghe Damsté, J.S., 2005. Identification of carotenals in sediments. Organic Geochemistry 36, 485–495.
Hoshino, Y., Nettersheim, B.J., Gold, D.A., Vinnichenko, G., van Maldegem, L.M., Bishop, C., Brocks, J.J., Gaucher, E.A., 2023. Genetics re-establish the utility of 2-methylhopanes as cyanobacterial biomarkers before 750 million years ago. Nature Ecology & Evolution. https://doi.org/10.1038/s41559-023-02223-5.
Hou, M., Qu, J., Zha, M., Swennen, R., Ding, X., Imin, A., Liu, H., Bian, B., 2022. Significant contribution of haloalkaliphilic cyanobacteria to organic matter in an ancient alkaline lacustrine source rock: a case study from the Permian Fengcheng Formation, Junggar Basin, China. Marine and Petroleum Geology 138, 105546.
Huang, W.-Y., Meinschein, W.G., 1976. Sterols as source indicators of organic materials in sediments. Geochimica et Cosmochimica Acta 40, 323–330.
Huang, W.-Y., Meinschein, W.G., 1979. Sterols as ecological indicators. Geochimica et Cosmochimica Acta 43, 739–745.
Kang, X., Hu, W., Cao, J., Wu, H., Xiang, B., Wang, J., 2019. Controls on reservoir quality in fan-deltaic conglomerates: insight from the Lower Triassic Baikouquan Formation, Junggar Basin, China. Marine and Petroleum Geology 103, 55–75.
Kenig, F., Sinninghe Damsté, J.S., Kock-van Dalen, A.C., Rijpstra, W.I.C., Huc, A.Y., de Leeuw, J.W., 1995. Occurrence and origin of mono-, di-, and trimethylalkanes in modern and Holocene cyanobacterial mats from Abu Dhabi, United Arab Emirates. Geochimica et Cosmochimica Acta 59, 2999–3015.
Köster, J., Volkman, J.K., Rullkötter, J., Scholz-Böttcher, B.M., Rethmeier, J., Fischer, U., 1999. Mono-, di- and trimethyl-branched alkanes in cultures of the filamentous cyanobacterium *Calothrix scopulorum*. Organic Geochemistry 30, 1367–1379.
Lee, K.Y., 1985. Geology of the Petroleum and Coal Deposits in the Junggar (Zhungaer) Basin, Xinjiang Uygur Zizhiqu, Northwest China. US Department of the Interior, Geological Survey.
Li, D., He, D., Sun, M., Zhang, L., 2020. The role of arc-arc collision in accretionary orogenesis: insights from ~320 Ma tectono-sedimentary transition in the Karamaili area, NW China. Tectonics 39 e2019TC005623.
Liu, S., Gao, G., Jin, J., Gang, W., Xiang, B., 2022. Source rock with high abundance of C_{28} regular sterane in typical brackish-saline lacustrine sediments: biogenic source, depositional environment and hydrocarbon generation potential in Junggar Basin, China. Journal of Petroleum Science and Engineering 208, 109670.
Lu, H., Sheng, G., Ma, Q., Lu, Z., 2011. Identification of C_{24} and C_{25} lanostanes in Tertiary sulfur rich crude oils from the Jinxian Sag, Bohai Bay Basin, northern China. Organic Geochemistry 42, 146–155.
Luo, G., Hallmann, C., Xie, S., Ruan, X., Summons, R.E., 2015. Comparative microbial diversity and redox environments of black shale and stromatolite facies in the Mesoproterozoic Xiamaling Formation. Geochimica et Cosmochimica Acta 151, 150–167.
Luo, G., Yang, H., Algeo, T.J., Hallmann, C., Xie, S., 2019. Lipid biomarkers for the reconstruction of deep-time environmental conditions. Earth-Science Reviews 189, 99–124.
Ma, D., He, D., Li, D., Tang, J., Liu, Z., 2015. Kinematics of syn-tectonic unconformities and implications for the tectonic evolution of the Hala'alat Mountains at the northwestern margin of the Junggar Basin, Central Asian Orogenic Belt. Geoscience Frontiers 6, 247–264.
McKirdy, D.M., Hahn, J.H., 1982. The composition of kerogen and hydrocarbons in Precambrian rocks. In: Holland, H.D., Schidlowski, M. (Eds.), Mineral Deposits and the Evolution of the Biosphere (Dahlem Konferenzen 1982). Springer-Verlag, Berlin, pp. 123–154.
Murphy, S.M.T.J., McCormick, A., Eglinton, G., 1967. Perhydro-β-carotene in the Green River Shale. Science 157, 1040–1042.
Naafs, B.D.A., Bianchini, G., Monteiro, F.M., Sánchez-Baracaldo, P., 2022. The occurrence of 2-methylhopanoids in modern bacteria and the geological record. Geobiology 20, 41–59.
Parfenova, T.M., 2011. Hydrocarbons of the lanostane homologous series in the Phanerozoic organic matter and their probable biologic sources. Russian Geology and Geophysics 52, 773–780.
Peng, P., Morales-Izquierdo, A., Fu, J., Sheng, G., Jiang, J., Hogg, A., Strausz, O.P., 1998. Lanostane sulfides in an immature crude oil. Organic Geochemistry 28, 125–134.
Peniguel, G., Couderc, R., Seyve, C., 1989. Les microalgues actuelles et fossiles: intérêt stratigraphique et pétrolier. Bulletin des Centres de Recherches Exploration-Production Elf-Aquitaine 13, 455–482.
Peters, K.E., 1986. Guidelines for evaluating petroleum source rock using programmed pyrolysis. AAPG Bulletin 70, 318–329.
Peters, K.E., Walters, C.C., Moldowan, J.M., 2005. The Biomarker Guide Volume 2: Biomarkers and Isotopes in Petroleum Systems and Earth History, Second Edition. Cambridge University Press, Cambridge.
Philp, R.P., Fan, Z., 1987. Geochemical investigation of oils and source rocks from Qianjiang Depression of Jianghan Basin, a terrigenous saline basin, China. Organic Geochemistry 11, 549–562.
Radke, M., 1983. The methylphenanthrene index (MPI): a maturity parameter based on aromatic hydrocarbons. Advance in Organic Geochemistry 1981, 504–512.
Requejo, A.G., Allan, J., Creaney, S., Gray, N.R., Cole, K.S., 1992. Aryl isoprenoids and diaromatic carotenoids in Paleozoic source rocks and oils from the Western Canada and Williston Basins. Organic Geochemistry 19, 245–264.
Ruble, T.M., Bakel, A.J., Philp, R.P., 1994. Compound specific isotopic variability in Uinta Basin native bitumens: paleoenvironmental implications. Organic Geochemistry 21, 661–671.
Sakata, S., Hayes, J.M., McTaggart, A.R., Evans, R.A., Leckrone, K.J., Togasaki, R.K., 1997. Carbon isotopic fractionation associated with lipid biosynthesis by a cyanobacterium: relevance for interpretation of biomarker records. Geochimica et Cosmochimica Acta 1997, 5379–5389.
Shiea, J., Brassell, S.C., Ward, D.M., 1990. Mid-chain branched mono-and dimethyl alkanes in hot spring cyanobacterial mats: a direct biogenic source for branched alkanes in ancient sediments? Organic Geochemistry 15, 223–231.
Shiea, J., Brassell, S.C., Ward, D.M., 1991. Comparative analysis of extractable lipids in hot spring microbial mats and their component photosynthetic bacteria. Organic Geochemistry 17, 309–319.
Sinninghe Damsté, J.S., Kenig, F., Koopmans, M.P., Köster, J., Schouten, S., Hayes, J.M., de Leeuw, J.W., 1995. Evidence for gammacerane as an indicator of water column stratification. Geochimica et Cosmochimica Acta 59, 1895–1900.
Summons, R.E., Franzmann, P.D., Nichols, P.D., 1998. Carbon isotopic fraction associated with methylotrophic methanogenesis. Organic Geochemistry 1998, 465–475.

Summons, R.E., Jahnke, L.L., Hope, J.M., Logan, G.A., 1999. 2-Methylhopanoids as biomarkers for cyanobacterial oxygenic photosynthesis. Nature 400, 554–557.
Summons, R.E., Bradley, A.S., Jahnke, L.L., Waldbauer, J.R., 2006. Steroids, triterpenoids and molecular oxygen. Philosophical Transactions of the Royal Society B: Biological Science 361, 951–968.
Talbot, H.M., Summons, R.E., Jahnke, L.L., Cockell, C.S., Rohmer, M., Farrimond, P., 2008. Cyanobacterial bacteriohopanepolyol signatures from cultures and natural environmental settings. Organic Geochemistry 39, 232–263.
Tang, W., Zhang, Y., Pe-Piper, G., Piper, D.J.W., Guo, Z., Li, W., 2021a. Permian rifting processes in the NW Junggar Basin, China: implications for the post-accretionary successor basins. Gondwana Research 98, 107–124.
Tang, W., Zhang, Y., Pe-Piper, G., Piper, D.J., Guo, Z., Li, W., 2021b. Permian to early Triassic tectono-sedimentary evolution of the Mahu sag, Junggar Basin, western China: sedimentological implications of the transition from rifting to tectonic inversion. Marine and Petroleum Geology 123, 104730.
Tao, K., Cao, J., Chen, X., Nueraili, Z., Hu, W., Shi, C., 2019. Deep hydrocarbons in the northwestern Junggar Basin (NW China): geochemistry, origin, and implications for the oil vs. gas generation potential of post-mature saline lacustrine source rocks. Marine and Petroleum Geology 109, 623–640.
ten Haven, H.L., de Leeuw, J.W., Sinninghe Damsté, J.S., Schenck, P.A., Palmer, S.E., Zumberge, J.E., 1988. Application of biological markers in the recognition of palaeohypersaline environments. Geological Society, London, Special Publications 40, 123–130.
ten Haven, H.L., Rohmer, M., Rullkötter, J., Bisseret, P., 1989. Tetrahymanol, the most likely precursor of gammacerane, occurs ubiquitously in marine sediments. Geochimica et Cosmochimica Acta 53, 3073–3079.
Tissot, B.P., Welte, D.H., 1984. Petroleum Formation and Occurrence, Second Edition. Springer Verlag, Heidelberg.
Wan, L., Liu, J., Mao, F., Lv, M., Liu, B., 2014. The petroleum geochemistry of the Termit Basin, Eastern Niger. Marine and Petroleum Geology 51, 167–183.
Wang, T., Cao, J., Carroll, A.R., Zhi, D., Tang, Y., Wang, X., Li, Y., 2021b. Oldest preserved sodium carbonate evaporite: Late Paleozoic Fengcheng Formation, Junggar Basin, NW China. GSA Bulletin 133, 1465–1482.
Wang, T., Cao, J., Jin, J., Xia, L., Xiang, B., Ma, W., Li, W., He, W., 2021c. Spatiotemporal evolution of a Late Paleozoic alkaline lake in the Junggar Basin, China. Marine and Petroleum Geology 124, 104799.
Wang, Y., Liu, L., Ji, H., Song, G., Wang, X., Sheng, Y., 2019. Structure of a pre-Triassic unconformity and its hydrocarbon transporting characteristics, Wuerhe-Fengnan area, Junggar Basin, China. Journal of Petroleum Science and Engineering 173, 820–834.
Wang, D., Zou, X., Li, M., Chen, G., Ma, C., Qin, H., 2021a. The detection and geochemical significance of C_{30}–C_{32} Lanostane from Permian alkaline source rocks in the Fengcheng Formation, in Wuerhe, Junggar Basin. Geochimica 50, 591–601.
Welander, P.V., Coleman, M.L., Sessions, A.L., Summons, R.E., Newman, D.K., 2010. Identification of a methylase required for 2-methylhopanoid production and implications for the interpretation of sedimentary hopanes. Proceedings of the National Academy of Sciences of the United States of America 107, 8537–8542.
Werne, J.P., Lyons, T.W., Hollander, D.J., Schouten, S., Hopmans, E.C., Sinninghe Damsté, J.S., 2008. Investigating pathways of diagenetic organic matter sulfurization using compound-specific sulfur isotope analysis. Geochimica et Cosmochimica Acta 72, 3489–3502.
Wieland, A., Pape, T., Möbius, J., Klock, J.H., Michaelis, W., 2008. Carbon pools and isotopic trends in a hypersaline cyanobacterial mat. Geobiology 6, 171–186.
Xia, L., Cao, J., Bian, L., Hu, W., Wang, T., Zhi, D., Li, E., 2022. Co-evolution of paleo-environment and bio-precursors in a Permian alkaline lake, Mahu mega-oil province, Junggar Basin: implications for oil sources. Science China Earth Sciences 65, 462–476.
Xiao, Z., Chen, S., Liu, C., Lu, Z., Zhu, J., Han, M., 2021. Lake basin evolution from early to Middle Permian and origin of Triassic Baikouquan oil in the western margin of Mahu Sag, Junggar Basin, China: evidence from geochemistry. Journal of Petroleum Science and Engineering 203, 108612.
Xie, S., Pancost, R.D., Yin, H., Wang, H., Evershed, R.P., 2005. Two episodes of microbial change coupled with Permo/Triassic faunal mass extinction. Nature 434, 494–497.
Xie, S., Pancost, R.D., Wang, Y., Yang, H., Wignall, P.B., Luo, G., Jia, C., Chen, L., 2012. Cyanobacterial blooms tied to volcanism during the 5 my Permo-Triassic biotic crisis. Geology 38, 447–450.
Yu, K., Cao, Y., Qiu, L., Sun, P., Jia, X., Wan, M., 2018. Geochemical characteristics and origin of sodium carbonates in a closed alkaline basin: the Lower Permian Fengcheng Formation in the Mahu Sag, northwestern Junggar Basin, China. Palaeogeography, Palaeoclimatology, Palaeoecology 511, 506–531.
Yu, Z., Wang, Z., Wang, J., Li, Z., 2022. Subtle reservoirs and implications for hydrocarbon exploration in terrestrial lacustrine fan-delta deposits: insights from the Triassic Baikouquan Formation, Mahu Sag, Junggar Basin, western China. Marine and Petroleum Geology 142, 105730.
Yu, K., Zhang, Z., Cao, Y., Qiu, L., Zhou, C., Cheng, D., Sun, P., Yang, Y., 2021. Origin of biogenic-induced cherts from Permian alkaline saline lake deposits in the NW Junggar Basin, NW China: implications for hydrocarbon exploration. Journal of Asian Earth Sciences 211, 104712.
Zhang, Z., Gu, Y., Jin, J., Li, E., Yu, S., Pan, C., 2022. Assessing source and maturity of oils in the Mahu sag, Junggar Basin: molecular concentrations, compositions and carbon isotopes. Marine and Petroleum Geology 141, 105724.
Zhang, Z.M., Liou, J.G., Coleman, R.G., 1984. An outline of the plate tectonics of China. GSA Bulletin 95, 295–312.
Zumberge, J.E., 1987. Terpenoid biomarker distributions in low maturity crude oils. Organic Geochemistry 11, 479–496.